Atmospheric impacts of local ocean grid refinement in a coupled earth system model

Jonny Williams[1], Erik Behrens[1], Vidya Varma[1*], Olaf Morgenstern[1], João Teixeira[2]

[1]National Institute of Water and Atmospheric Research (NIWA), Hataitai, Wellington, New Zealand
[2]Met Office, Fitzroy Road, EX1 3PB, Exeter, UK

Key Points:

- Embedding a high resolution regional ocean model into a global earth system model has important effects on local and hemispheric climate.
- Compared to when the grid is the same everywhere, the air temperature over the high resolution region is improved compared to observations.
- Changes to cloud reflectivity over the Southern Ocean are significantly improved compared to a fixed-grid-size control ensemble.

*Now at Institut für Geophysik und Meteorologie, Universität zu Köln, Pohligstraße 3, 50969 Köln, Germany

Corresponding author: Jonny Williams, jonny.williams@niwa.co.nz

Abstract

We report the results of two Earth System Model (ESM) configurations which differ in their ocean physics around New Zealand. The first is a global low-resolution configuration of UKESM1.0 while the second model, NZESM has an eddy-permitting ocean embedded around New Zealand. The nominal ocean resolution of the UKESM is 1°and that of the NZESM is 0.2°.

Near New Zealand, total cloud amount is negatively correlated with temperature. This relationship is reversed near the seasonal sea ice edge where increased evaporation results from open ocean which was previously covered in sea ice.

In the simulations, the change to the cloud amount is dominated by changes to stratocumulus cloud and the resulting improvement to shortwave cloud radiative effect - with respect to CERES-EBAF observations - is statistically significant at the 95% level across the Southern Ocean, assuming a normally distributed control ensemble. The near-surface air temperature in the vicinity of the nested ocean model is also improved, when compared to ERA5 reanalysis data.

In general, clouds and their radiative effects over the Southern Ocean are not well simulated by Earth System Models and the changes made here improve both near-surface temperature near New Zealand and zonal mean shortwave cloud radiative effect across the Southern Ocean. Noting that the development of climate models always involves an element of 'tuning', changing the regional ocean physics without doing any further tuning (as is the case here), will tend to remove some compensating bias and therefore make the model-observation agreement in some regions less good.

Plain Language Summary

We compare two global climate models, one which has a high resolution ocean model in the New Zealand region, and one that is about 1° everywhere

Near New Zealand, the total amount of cloud goes down when the temperature goes up but this is reversed closer to the South Pole. This is because as the temperature goes up near Antarctica, more evaporation from the sea surface happens because the sea surface isn't covered in ice any more.

Compared to a model where the ocean grid is the same everywhere, we find that the air temperature is in better agreement with observations in this region. We also observe that changes to cloud reflectivity over the Southern Ocean are significantly improved and this is mostly due to changes in low level, medium thickness clouds called stratocumulus.

Because climate models are so complex - often involving hundreds of thousands of lines of code - it is usually necessary to 'tune' some of the model parameters. This tends to introduce errors which cancel each other out. In this case we have done no additional tuning and so therefore some aspects of the climate are expected to get worse, and this is indeed observed in some areas.

1 Introduction

Earth System Models - ESMs - are complex and computationally intensive pieces of software for understanding past climates and informing projections of future ones. A single simulation can use thousands of computer processors and can easily generate tens or hundreds of terabytes of data, e.g. Eyring et al. (2016).

The New Zealand Earth System Model - NZESM (Williams et al., 2016; Behrens et al., 2020) - is a modified version of the low-resolution configuration of the United Kingdom Earth UKESM1.0 (Sellar et al., 2020). The physical oceanography of the NZESM is described in detail in Behrens et al. (2020), the only difference to the UKESM is the inclusion of an embedded high-resolution ocean model in the New Zealand region. This is discussed in more detail below.

Climate models' representation of Southern Ocean climate is subject to some notable biases. The Southern Ocean warm bias is arguably the most prominent one, however there are associated biases in cloud properties and - concomitantly - in their radiative effects (Sallée et al., 2013; Kay et al., 2016; Bodas-Salcedo et al., 2016).

Several authors have documented Southern Ocean model bias, as well as the mechanisms that contribute to them (Hyder et al., 2018; Varma et al., 2020; Bodas-Salcedo et al., 2012). For example, Hyder et al. (2018) demonstrated that Southern Ocean model-observation mismatches can be interpreted as being due to shortwave radiation biases in the clouds and surface radiation fields. Varma et al. (2020) study cloud microphysics – specifically the shape of ice crystals in the atmosphere – and find that relaxation of the traditional assumption of spherical crystals yields an improvement of up to 4 Wm^{-2}. In contrast, Bodas-Salcedo et al. (2012) study the effect on surface radiation biases due to cloud biases in cyclone systems, developing a new clustering method and showing that the resulting biases are mostly due to the mid and low level clouds in the cold air sector of the cyclones.

The studies above consider atmosphere-only GCMs but ocean-only and coupled models have also been used to investigate this longstanding bias. For example, Hawcroft et al. (2016) examine the HadGEM2-ES coupled model, results from which were submitted to the 5th Coupled Model Intercomparison Project (CMIP5; Taylor et al., 2012). This study discusses the origin of the model's bias in detail and describes the effects of corrections to the albedo over the Southern Ocean on - for example - atmospheric jets and the 'double ITCZ' problem (e.g. see Tian & Dong, 2020, for a review).

From the perspective of ocean-only models, Tsujino et al. (2020) provide a detailed overview of the basis and findings of the second phase of the Ocean Model Intercomparison Project (OMIP-2). More specifically, Chassignet et al. (2020) examines the role of horizontal grid resolution and finds that although some fields are consistently improved as resolution increases - western boundary, equatorial and Antarctic circumpolar currents - some are degraded in some models, e.g. temperature and salinity profiles.

It is beyond the scope of this work to give a detailed review of our understanding of the Southern Ocean biases present in coupled climate models; something that is persistent and widespread in coupled models from CMIP5 and CMIP6. The UKESM is a complex coupled earth system model, and its varied processes are documented across many publications.

Southern Ocean biases in coupled climate models are two-fold, manifesting in a persistent surface warm bias of the Southern Ocean (e.g. Yool et al. (2021) §3.1) and in a large shortwave cloud radiative effect - SWCRE - bias in the same region (e.g. Varma et al. (2020) §3). In coupled models these biases are inherently connected, and this study exhibits changes to both biases even though the atmosphere component in the two model configurations studied is identical.

2 Models and datasets

2.1 Model description of the NZESM

The atmospheric component of the models used here is the 'Global Atmosphere Model, Version 7.1', or GA7.1 (Walters et al., 2019). It uses a semi-implicit semi-Lagrangian dynamical core (Wood et al., 2014), the SOCRATES radiation scheme, based on Edwards and Slingo (1996), shallow and deep mass-flux-based convection - e.g. (Gregory & Rowntree, 1990) - and sub-gridscale boundary layer turbulence - e.g. Brown et al. (2008). The NZESM simulates explicit tropospheric and stratospheric chemistry (Archibald et al., 2020).

With particular reference to the subject matter of this manuscript, clouds in the NZESM and UKESM are described by Wilson et al. (2008) and Wilsön et al. (2008) and their inclusion into the atmospheric component of the UKESM is described in Walters et al. (2019). In this scheme, cloud condensate *and* cloud fraction are prognostic variables; that is, they are calculated 'online' within the equation system solved by the model code. This improves on the previous 'diagnostic' scheme used in weather and climate forecasting codes used by members of the Unified Model Partnership (Brown et al., 2012) by more realistically linking water vapour, condensate, and cloud fraction amounts.

The ocean model configuration - including a detailed description of the Southern Ocean - used by the models is documented in Storkey et al. (2018) and Yool et al. (2021) and is known as 'Global Ocean Model, Version 6', or GO6. Compared to the previous iteration of the 'GO' family of models, GO6 shows multi-variable improvements in the Southern Ocean region which are attributed to changes in ocean mixing parameter values. The coupling between the different model components is done via the OASIS coupler, which is used in several CMIP6-standard models (Craig et al., 2017).

The physical basis model (coupled ocean-atmosphere-sea ice but without the full biogeochemical complexity) of the UKESM is called HadGEM3-GC31-LL (Kuhlbrodt et al., 2018). This model exists in two resolutions, N96ORCA1 (the parent resolution of the NZESM) and N216ORCA025 and the former exhibits a smaller overall Southern Ocean warm bias due to improved volumetric ACC transport and a higher fidelity annual sea ice cycle.

The overall UKESM climatology is described in Sellar et al. (2019), detailed study of the aerosol scheme in this family of coupled models is given in (Mulcahy et al., 2020).

Looking ahead, Varma et al. (2020) describe improvements to the Southern Ocean cloud-albedo bias in an atmosphere-only configuration of GA7.1; the atmosphere component of the UKESM. The cloud scheme improvements relate to shape of ice crystals and may be included in a future configuration of the NZESM.

2.2 Eddies and resolution mismatches

The NZESM includes a two - way nested, high - resolution ocean version of the GO6 model in the New Zealand region whilst keeping all other aspects of the ocean model unchanged. This nesting has been achieved using the Adaptive Grid Refinement In Fortran – AGRIF – method (Debreu et al., 2008) and has increased the nominal ocean grid resolution from 1° to 0.2°; thus achieving a 25 fold increase in areal mesh density. The physical oceanography of the UKESM/NZESM model pair is described in (Behrens et al., 2020) and the nested region is illustrated in Figure 1. This study uses the same two simulations considered there but analyses them from an atmosphere - ocean - sea ice perspective.

Behrens et al. (2020) showed that sea surface temperatures - SSTs - in the region surrounding New Zealand are improved with respect to observations because of the bet-

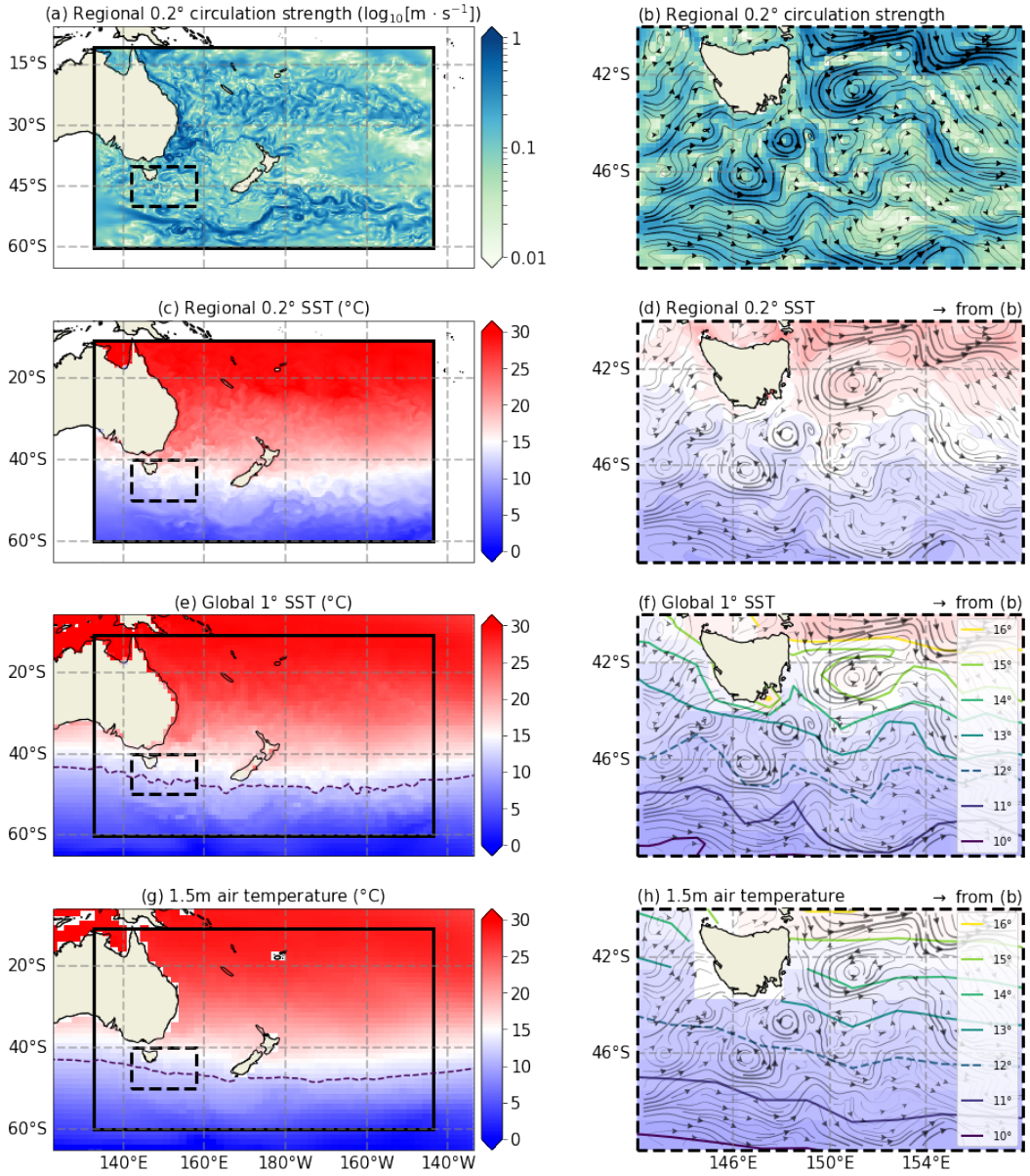

Figure 1. (a) Surface ocean circulation speed of the 0.2° nested ocean model. (b) As for (a) but zoomed into the dashed area and including vector streamlines with widths proportional to speed. (c) Sea surface temperature of the nested 0.2° ocean model. (d) As for (c) but zoomed into the dashed area and including the streamlines from (b). (e) Sea surface temperature from the 1° global ocean model. The 12° isotherm is included to illustrate the increase in spatial 'noisiness' in the nested ocean region. (f) As for (e) but zoomed into the dashed area and including the streamlines from (b). Contours are at the same levels as the background colours and are intervals of 1°C from 10°C to 16°C and are described by the legend. The 12°C contour is dashed to assist comparison with (e). (g) 1.5m air temperature at 1.25°×1.875°. The 12°C isotherm is included as in (e). (h) As for (g) but zoomed into the dashed area and including the streamlines from (b). The 12° contour is dashed to assist comparison with (e). All sub-Figures on the same horizontal level have the same colour limits as indicated by the appropriate colour bar. All data is for the mean of January 1989.

ter representation of ocean currents which the finer ocean grid allows. In particular, the transportation of heat and water volumes in the vicinity of the Tasman Front and the East Australian Current are improved which in turn improve the SST; indeed as Behrens et al. (2020) state:

> '*... the air-sea fluxes of heat and moisture over the [Tasman Sea] can be considered a pacemaker for New Zealand's weather and climate*'.

Since this work and that of Behrens et al. (2020) use multi-decadal means, this improvement to the SSTs in the absence of any changes to the atmospheric physics means that near-surface air temperature comes into equilibrium with the sea surface and improves its agreement with reanalysis data.

Even at a resolution of 0.2° the nested region resolution is still not high enough for the model to be considered 'eddy resolving', it *is* high enough to be 'eddy permitting'. This distinction is described in detail in e.g. J. He et al. (2018). Although the nested high-resolution ocean model is run around New Zealand, the coarser global-ocean model is also run in the same region. It is this lower-resolution model which is coupled to the atmosphere, and hence the detailed eddy-resolving structure of the underlying high-resolution ocean model is not passed to the atmosphere directly, but via a lower resolution intermediary.

Figure 1 illustrates how the eddy activity in the nested ocean model is related to the air temperature. Figure 1(a) and (b) show the nested ocean's surface circulation speed at different length scales; the entire high-resolution region, and zoomed in to a particularly active eddy region south and west of Tasmania. (b) also shows circulation streamlines and these are also included in (d,f,h) to aid interpretation. The 2$^{\text{nd}}$ row - sub-Figures (c) and (d) show the sea surface temperature for the nested model. The 3$^{\text{rd}}$ row shows the SST in the same region but for the global, 1°, ocean model. (f) shows the zoomed in colours from (e) as well as contour levels at integer temperature values. Finally, the 4$^{\text{th}}$ row shows analogous sub-Figures as for the 3$^{\text{rd}}$ but for atmospheric temperatures.

There are two resolution mismatches to be considered here: (1) 0.2° nested ocean to 1° global ocean to; (2) 1° global ocean to 1.25°×1.875° atmosphere. The coupling between the ocean models is two-way but spatial information will naturally be lost in the upscaling procedure. That said, the evidence of the 'fingerprint' of the nested ocean on the global ocean model is clearly visible by comparing the SST field in Figure 1(e) inside and outside the nested region. This is even visible in the 1.5m air temperature, particularly around the northern reaches of the Antarctic Circumpolar Current at approximately 50°S and in the southward depression of the isotherms around 151°E in (h).

2.3 Validation datasets and metrics

We compare 20-year annual and seasonal means (1989-2008) of climate model output to observational and reanalysis products of temperature, total cloud amount, stratocumulus amount, and shortwave cloud radiative effect (SWCRE). The models runs are started in 1950 to enable model spin-up to occur and both models start from initial conditions from UK Met Office suite ID `u-bb075` (Tang et al., 2019), which was itself run from 1850. All spatial data considered here is regridded to the native atmosphere model gridscale of 1.25°×1.875°. This is the so-called 'N96' model resolution Mulcahy et al. (2020).

The simulated 1.5m temperatures are compared to the 2m temperatures from the state-of-the-art ERA5 reanalysis Hersbach et al. (2020).

For total and stratocumulus cloud amounts we use the output from the International Satellite Cloud Climatology Project, ISCCP (W. B. Rossow & Schiffer, 1999; W. Rossow & Duenas, 2004), and for the shortwave cloud radiative effect, data from the Energy Bal-

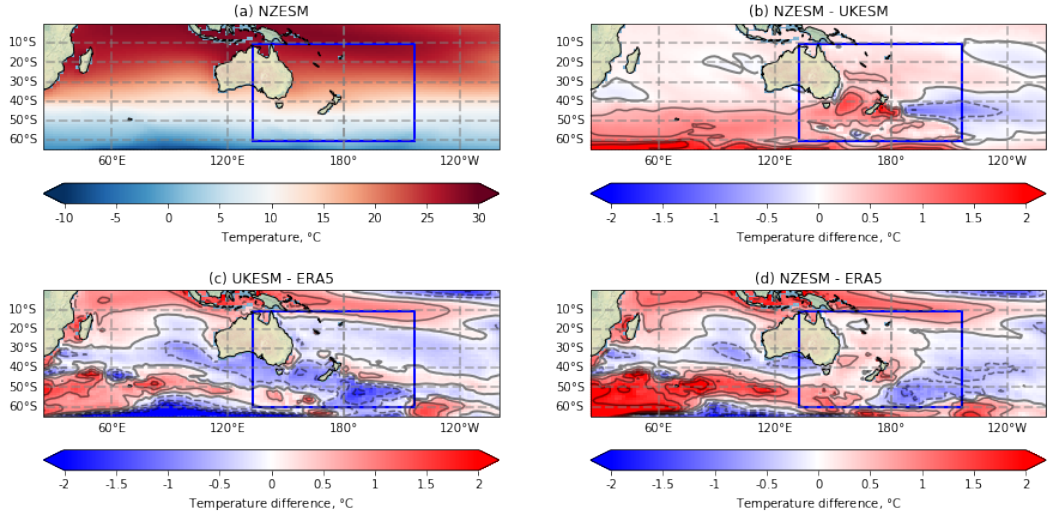

Figure 2. Near-surface annual mean air temperature (°C) for: (a) NZESM (b) NZESM - UKESM; (c) NZESM - ERA5 reanalysis; (d) UKESM - ERA5 reanalysis. All data is for 1989-2008.

anced and Filled product from the Clouds and the Earth's Radiant Energy System project; CERES - EBAF (Loeb et al., 2018) for the available period of 2000-2018. We concentrate on the shortwave radiation biases in the models since this is a particularly prevalent issue in present-day models. This is covered in some detail in Varma et al. (2020) and references therein.

For sea ice edge and concentration data, we use the HadISST dataset of Rayner et al. (2003).

3 Results

3.1 Temperature

Figure 2 shows annual mean 1.5m air temperature for the UKESM and NZESM compared to ERA5 reanalysis data (Hersbach et al., 2020) for the period 1989-2008. We can compare the atmosphere data shown in Figure 2 with equivalent ocean data in Behrens et al. (2020) - hereafter EB20. Figure 2(b) is analogous to Figure 9(a) in EB20 (reformatted here in Figure 3) and Figures 2(c-d) are analogous to Figures 8(a-b) in EB20 (reformatted here in Figure 4).

The region defined by the blue rectangle in 2 denotes the location of the high-resolution nested ocean model. From here we refer to this as the AGRIF region, named after the method used to implement this change (Behrens et al., 2020; Behrens, 2020; Debreu et al., 2008).

As noted above in section 2.2 there is less spatial variability - i.e. it is more homogeneous - in the atmosphere temperature field than in the equivalent ocean field in EB20. This is because of the lower resolution of the atmosphere model compared to the high-resolution nested ocean model.

The ocean data in EB20 uses the EN4 climatology (Good et al., 2013) for sea surface temperature and therefore this serves as a useful counterpoint to previous analyses with a difference 'ground truth' dataset. Overall, the agreement with the ERA5 re-

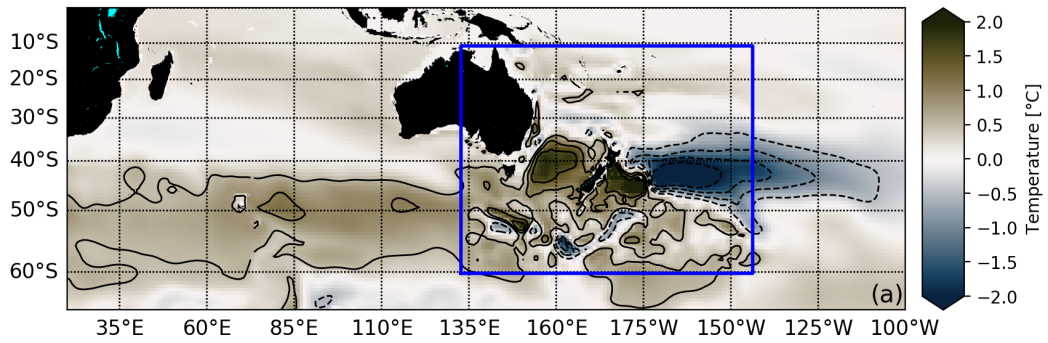

Figure 3. reformatted data – Figure 9(a) – from EB20. This is the ocean near-surface (0 - 500m) analogue of Figure 2(b) but for 1995-2014.

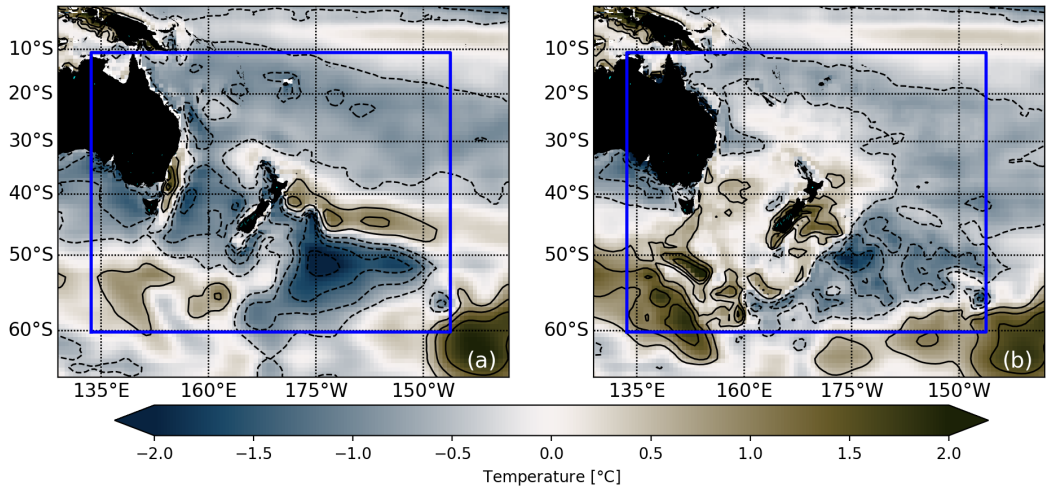

Figure 4. reformatted data – Figures 8(a-b) – from EB20. This is the ocean surface analogue of Figure 2(c-d) but for 1995-2014.

analysis is better in the NZESM compared to the UKESM, particularly in the vicinity of the AGRIF region although it should be noted that this is not the case universally.

For example, in the south western Indian Ocean, the warm bias is exacerbated and this is accompanied by an improvement in the cold bias seen in the south eastern portion. We shall see in the next section however that these temperature effects are accompanied by significant improvements to clouds and radiation. This improvement-deterioration pair is often encountered in climate model development but it should be noted that we are presenting the behaviour as observed when the global ocean model physics is changed, rather than presenting the results of a tuning exercise. The tuning of climate models indeed has its own literature and the interested reader is referred elsewhere (Schmidt et al., 2017; Hourdin et al., 2017; McNeall et al., 2020).

3.2 Total cloud amount

Before moving on to study clouds and radiation in more detail, it is instructive to compare the total cloud amount from the models to the data from the widely-used International Satellite Cloud Climatology Project, or ISCCP (W. B. Rossow & Schiffer, 1999; W. Rossow & Duenas, 2004). Since different satellites use different instruments and retrieval algorithms it is important to compare like with like. To achieve this, we use cloud amount output from the COSP simulator package in the models - e.g. Swales et al. (2018).

Figure 5 shows the total cloud amount for the models and ISCCP. It also shows the 15% contour of the September Antarctic sea ice amount. This will be discussed at length below. The rationale of using 15% as a measure of extent is discussed in (Kwok & Rothrock, 2009).

The difference between the simulated cloud amounts for the models (Figure 5(b)) is much smaller than the difference between the models and ISCCP itself. This is expected since the atmospheric physics of the models is identical. We expect some differences between the models due to the temperature differences noted above, but a large-scale change to the overall regional cloud amount would likely be spurious.

Overall, the cloud amount in this region does a reasonable job reproducing the spatial distribution of total cloud, although too much of it. Note however that the satellite swatch is clearly visible in the ISCCP data with values differing by ∼10% either side of it, for example, to the east of Madagascar.

Also, it is striking that the total cloud amount is negatively correlated with temperature in the region surrounding New Zealand (Figure 2(b), Figure 5(c)) but it is positively correlated at higher latitudes; specifically near the seasonal sea ice edge at ∼ -60° S.

3.3 Morphological cloud types

3.3.1 Annual mean

We will examine the temperature-cloud relationship in detail below but for now we will move on to partitioning the clouds into different bins defined by their cloud-top-pressure and optical depth or 'thickness'. We use 9 bins, as is frequently done in the literature, for example Mace et al. (2011).

Figure 6 shows the annual mean ISCCP cloud top height-optical depth bins for the NZESM and shows that the dominant cloud type in the Australia-New Zealand sector is stratocumulus - `Sc` for short - which occurs 14% of the time. The next most frequently occurring type is altostratus; occurring just over half as much of the time as `Sc`.

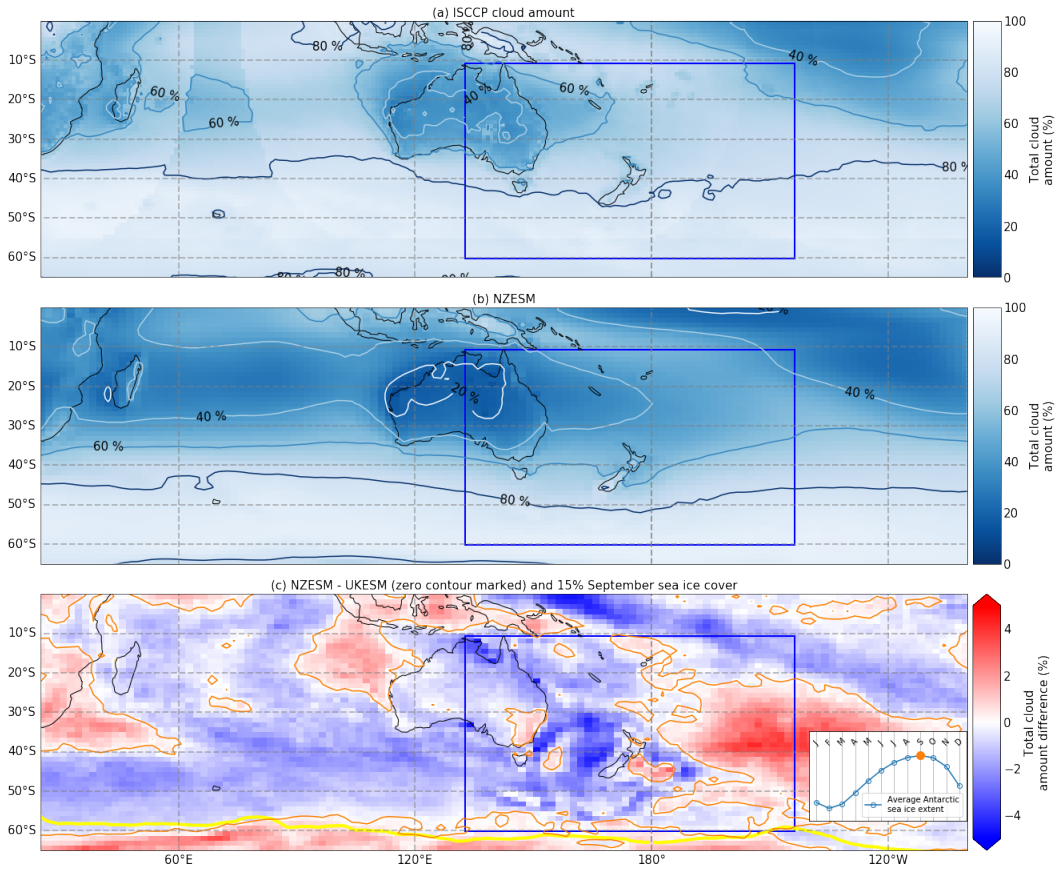

Figure 5. ISCCP total cloud amounts for (a) UKESM, (b) NZESM and (c) NZESM - UKESM. In (c) only the contour at zero is marked. The blue inset box shows the extent 'AGRIF' region. This box is present throughout the figures in this work. The yellow contour in (c) shows the 15% contour of the 20 year mean of September sea ice coverage from the HadISST dataset (Rayner et al., 2003) and the inset shows the seasonal cycle itself, showing September as the maximum.

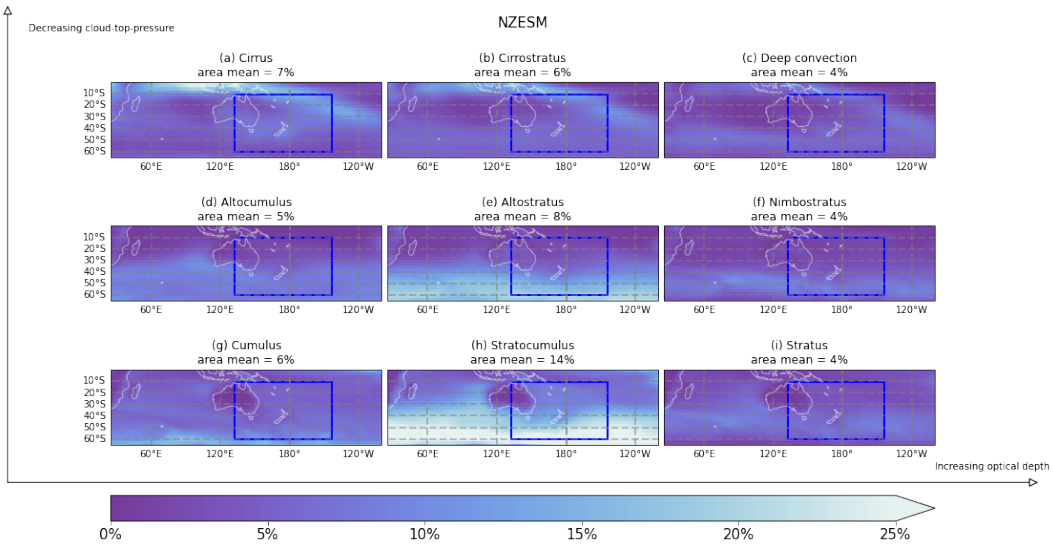

Figure 6. The nine ISCCP-D2 cloud types for the NZESM with their approximately-analogous morphological types. The x and y 'axes' indicate increasing optical depth and decreasing cloud-top-pressure respectively. The fractional coverage of each cloud type is given in the sub-figure titles.

However, when we examine the difference in these 9 types as simulated by the two models, then we see that it is only the Sc cloud type which is substantially different between the two model runs. Indeed, in the region of interest, there are virtually no differences greater than 1% and so we ignore these differences going forward and concentrate on Sc. Figure 7(a) shows the annual mean temperature differences for the models (as in 2(b)) and 2(b) shows the Sc differences.

Figure 7 shows that increased Sc amount is negatively correlated with temperature around the AGRIF region and that the sign of this correlation is reversed at higher latitudes. This reversal of correlation from negative (Sc$\sim$-T) to positive (Sc$\sim$T) at higher latitudes clearly correlates strongly with position of the sea ice edge (the yellow lines in Figure 7). The NZESM is warmer at higher southern latitudes and this is relfected in the southward movement of the sea ice edge. We examine this in detail below. We shall refer to these correlations as the r^- and r^+ regimes respectively going forward.

All the data considered thus far have been annual means over the 20 year period of 1989-2008. We now move on to consider the seasonal cycle of the Sc amount with respect to the air temperature and sea ice edge.

3.3.2 DJF

Figure 8 shows the December-January-February - DJF, austral summer - equivalent of 7.

The r^- regime around the AGRIF region remains clear in Figure 8 but the magnitude and extent of the temperature and Sc changes are reduced around the sea ice edge. We can immediately attribute this to the reduced sea ice amount in DJF and therefore the Sc amount clearly sensitive to the open ocean fraction. Note that the air temperature difference in and around the AGRIF region is essentially the same as in the annual mean case

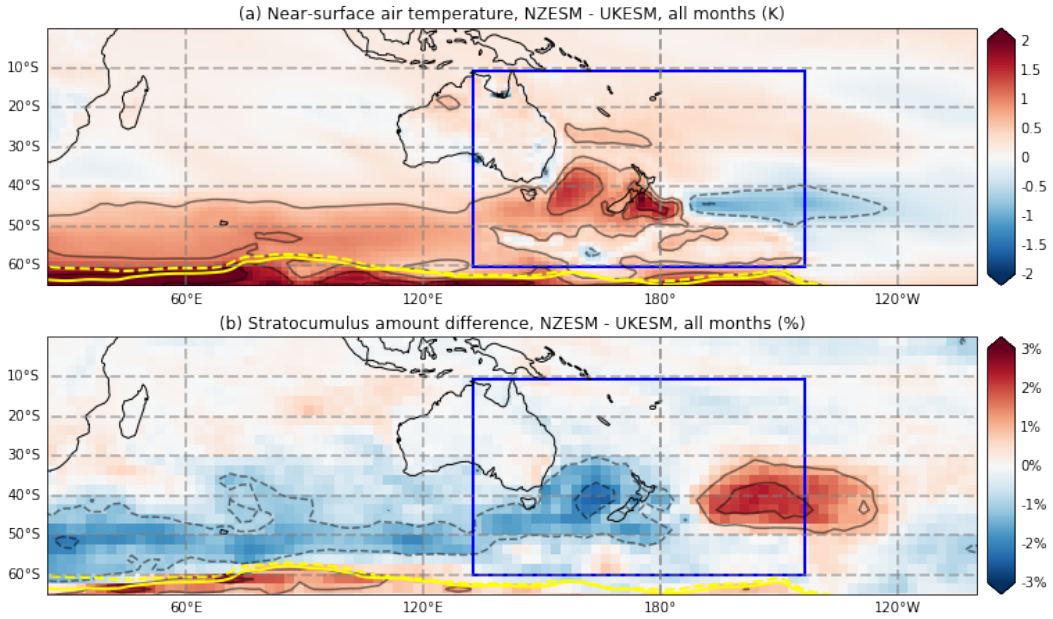

Figure 7. ISCCP-D2 percentage difference between the NZESM and UKESM. Only the Sc cloud type is shown here since all other morphological types show negligible differences. The yellow contours are the 15% contours for the annual mean sea ice concentration UKESM (dashed lines) and the NZESM (solid lines).

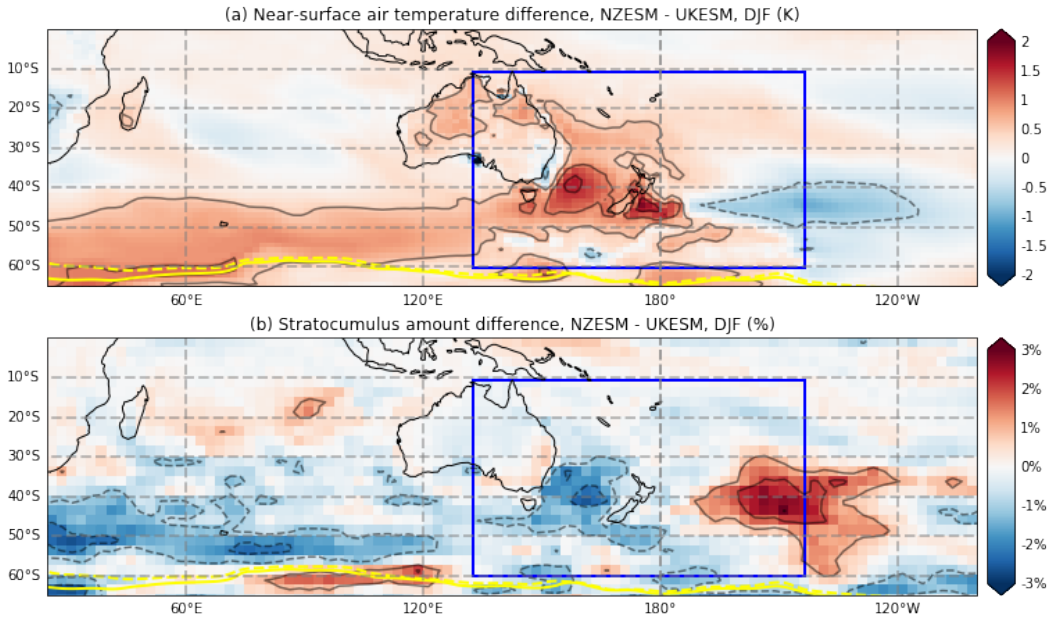

Figure 8. ISCCP-D2 percentage difference between the NZESM and UKESM, DJF.

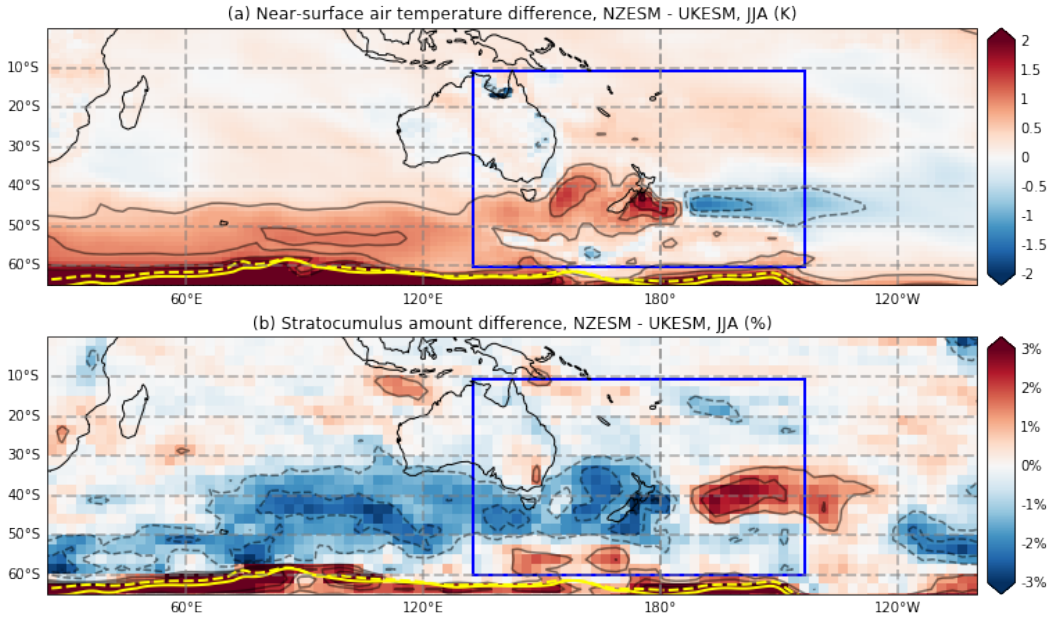

Figure 9. ISCCP-D2 percentage difference between the NZESM and UKESM, JJA.

It is somewhat counterintuitive that the position of the 15% sea ice concentration contour is seemingly so static (see Figure 9 also). However this is something of an artefact of the contour line chosen and the volume of ice throughout the year varies much more noticeably.

3.3.3 JJA

Figure 9 shows the June-July-August - JJA, austral winter - equivalent of 7.

In contrast to Figure 8, the air temperature difference around the sea ice edge is larger in JJA cf. the annual mean and this has the effect of amplifying the `Sc` differences seen in the annual mean. This is around the time when Antarctic sea ice is at its maximum and hence changes to the ice edge have a much more pronounced impact on the air-sea fluxes of moisture and heat, thus affecting the cloud formation. We note again that in the vicinity of the AGRIF region, the inter-model temperature difference is virtually identical to the annual mean value.

In the next section, we move on to examine the effect of cloud amount changes to the radiation budget over the Southern Ocean.

3.4 Shortwave cloud radiative effect - SWCRE

Shortwave cloud radiative effect—SWCRE—at the top of the atmosphere is defined as the difference between clear sky and all sky fluxes. The former only includes situations when clouds are absent and so this definition allows the effects of clouds to be isolated.

Figure 10 shows the SWCRE for the models compared to the CERES-EBAF dataset (Clouds and the Earth's Radiant Energy System - Energy Balanced and Filled) (Loeb et al., 2018).

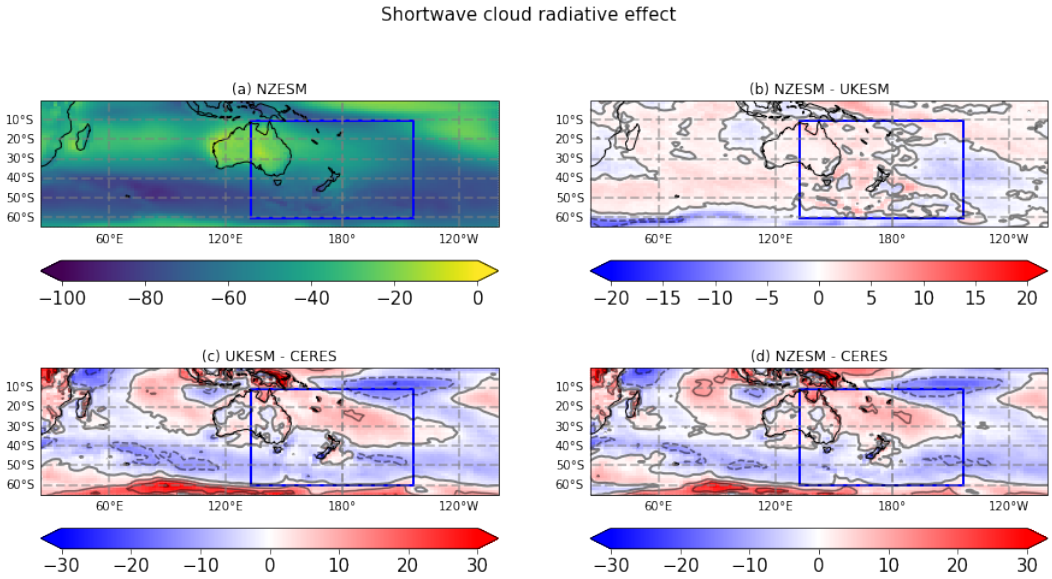

Figure 10. Shortwave cloud radiative effect for: (a) NZESM; (b) NZESM - UKESM; (c) UKESM - CERES; (d) NZESM - CERES. In (b-d), the contour spacing is 10 $W{\cdot}m^{-2}$ and the contour lines are solid and dashed for positive and negative values respectively.

Comparing Figure 10(b) and Figure 7(b) shows that increased Sc is associated with reduced shortwave cloud radiative effect, and vice versa. This is because the UKESM does not reflect as much shortwave radiation back to space as is observed. Therefore, increasing the amount of Sc increases reflection and so reduces the shortwave cloud radiative effect bias (Varma et al., 2020).

It is clear now that the change to the SWCRE is dominated by the Sc amount due to the striking correlation between ISCCP total cloud amount (Figure 5(c)), Sc amount (Figure 7(b)) and SWCRE (Figure 10(b)).

3.5 Zonal mean SWCRE against CERES observations

To examine the wider implications of these changes, we now take the zonal mean of these quantities over the entire Southern Ocean, which we define as that from 60° southward.

The results for the NZESM, UKESM and 16 member UKESM historical ensemble spread (Tang et al., 2019) are shown in Figure 11. The solid lines are for the NZESM results, the dashed lines for the UKESM run locally and the shaded regions are for a 16 member UKESM ensemble run at the UK Met Office.

For JJA, the agreement between the models and the observations is good but the DJF agreement is poor, peaking at over 30 $W \cdot m^{-2}$ on a background - NZESM value of $\approx 70W \cdot m^{-2}$ (Figure 10(a)).

It is particularly encouraging however that Figure 11 shows clearly that the bias is reduced in DJF and that the NZESM lies outside the shaded 2 standard deviation limits away from the ensemble mean. Therefore, assuming normally — i.e. Gaussian — distributed UKESM data, there is only a ≈5% chance that NZESM result is drawn from the same distribution as the UKESM. This gives confidence that this improvement is not due to natural variation, but rather to a statistically significant improvement in model

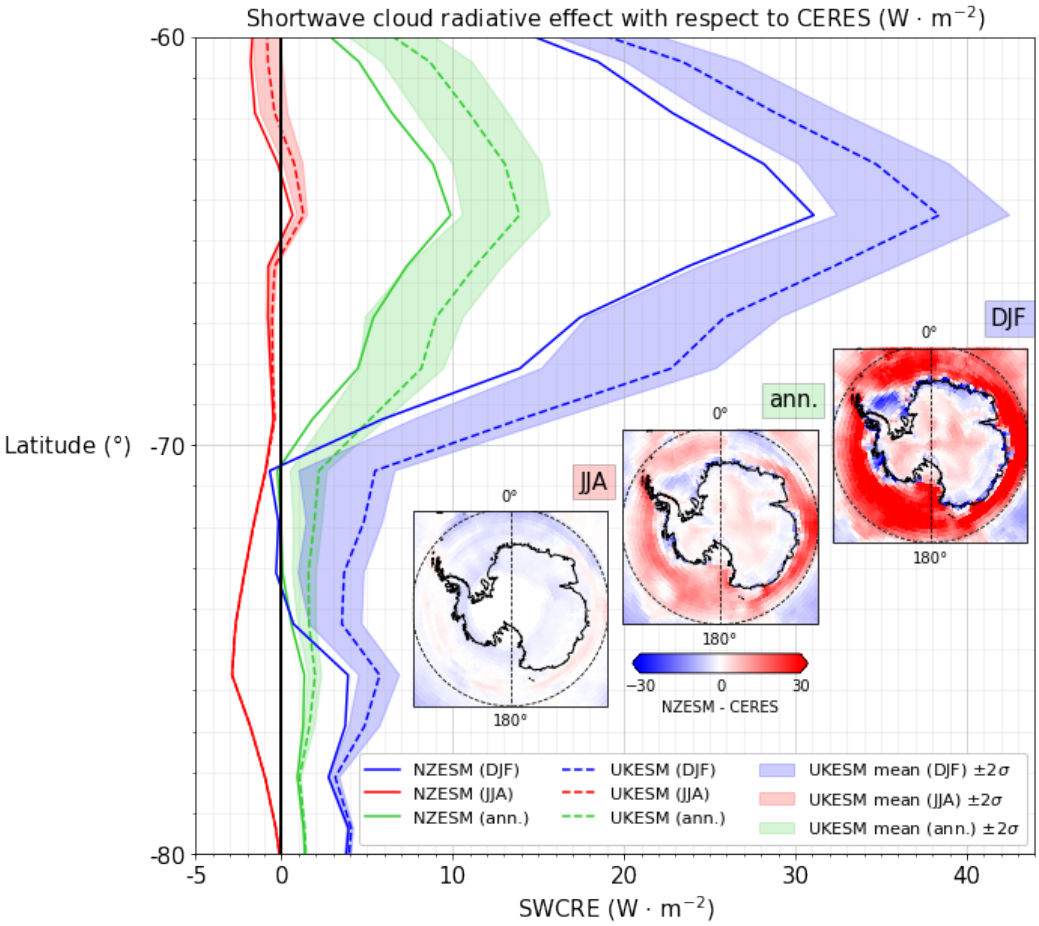

Figure 11. SWCRE differences between models and CERES observations. The main figure shows the NZESM, the UKESM and the UKESM ensemble mean in DJF, JJA and the annual means. The shaded region around each dashed line uses the ensemble mean ± 2 standard deviations (σ) from the UKESM historical ensemble. The inset maps show the SWCRE difference between the NZESM and CERES for the different meaning periods and using the same units. The 60° latitude line is marked as a dashed circle.

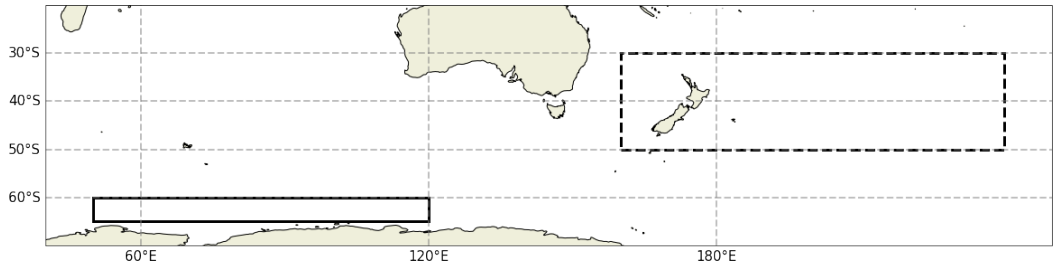

Figure 12. Regions examined in more detail in Figures 13(a) - dashed line box - and Figure 13(b) solid line box.

behaviour. This is brought about by improvements to the ocean physics in the NZESM which are then communicated to the atmosphere via the OASIS coupler.

3.6 NZESM Temperature versus stratocumulus amount regimes

As noted above, temperature and `Sc` amount are not correlated in the same direction across the region of interest. This is evident for example in Figure 7 which shows negative a negative correlation in and around the AGRIF region and a positive correlation near the sea ice edge.

In this section, we zoom in to two regions to examine these correlations in more detail for NZESM data and these are shown in Figure 12. South of ≈ -60°S, there is seasonal sea ice and the 15% contour of the simulated September maximum extent are shown in Figure 12. We have already seen in Figure 7 that as the sea ice edge retreats southward with increased temperature, this retreat is correlated with increased `Sc` amount and decreased SW cloud radiative effect (Figure 10(b)).

This reversal of the correlation between surface temperature and cloud amount tells us that there are different dominant physical mechanisms at play between these regions. This is to be expected since the surface boundary conditions are fundamentally different in each regime. In the negative correlation regime, the surface is entirely ice free all year round, whereas in the positive correlation regime, not only does the sea ice amount change throughout the year, but it is different between the two models. As mentioned above, we label these regimes r^+ and r^-, where in r^+, `Sc` $\sim T$ and in r^-, `Sc` $\sim -T$.

The r^- regime, has been previously discussed in Kawai et al. (2017) who note a general negative correlation between (ice free) SST and 'low stratiform cloud cover', LSC. Their definition of LSC includes `Sc`, stratus and 'sky-obscuring fog' whereas here we only consider `Sc`. However, we know from Figure 7 that the inter-model changes in cloud amount is dominated by `Sc` and so we assume that the comparison with the findings of Kawai et al. (2017) remain valid over open ocean in this study. The argument in Kawai et al. (2017) is based on considerations of entrainment at the cloud top combined with a modified lower-tropospheric stability index (Klein & Hartmann, 1993).

On the other hand, Huang et al. (2019) (and reference therein) show a positive correlation between Arctic sea ice decline and increased cloud cover - i.e. r^+ - due to increased evaporation from the ocean surface as the sea ice retreat.

Figure 13(a) illustrates the r^- regime where the `Sc` amount decreases as temperature increases. It shows model data and the range of the data from the case studies considered in Kawai et al. (2017). Values are scaled so that the `Sc` amount is zero at 0°C in all cases. The cloud amounts found in the model data at lower temperatures are lower

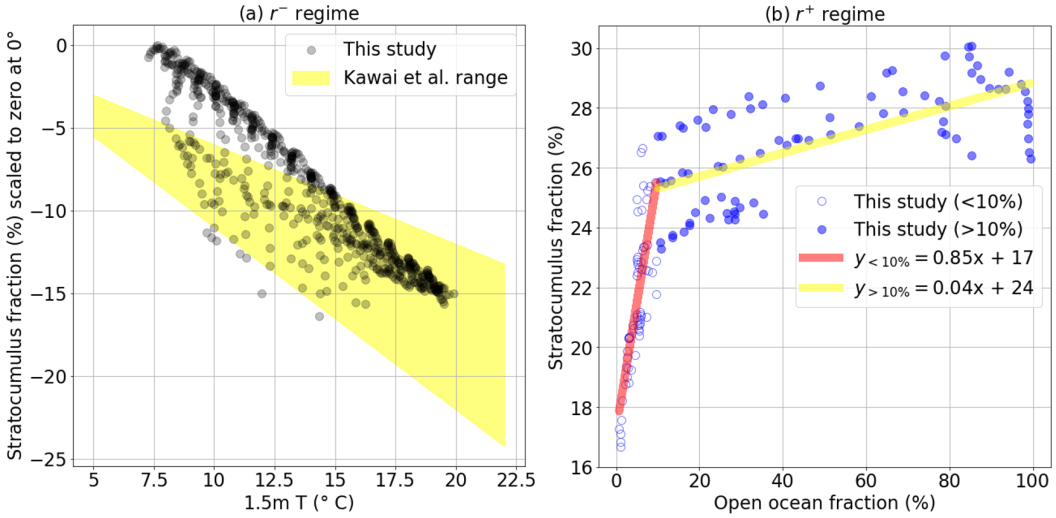

Figure 13. (a) Annual mean NZESM model data in the r^- regime showing the decrease in `Sc` fraction as temperature increases. The regions considered are shown by the dashed box in Figure 12. The blue dots are the model data, the red line is a linear fit to the model and the yellow shaded region shows the data from the case studies in Kawai et al. (2017). All data is scaled such that `Sc` is zero at $T = 0$ and the x-axis is expanded to aid comparison with Figure 14. (b) Model data in the r^+ regime showing the increase in `Sc` fraction as the open ocean fraction increases (i.e. as the temperature increases). The region considered is shown by the solid box in Figure 12). Note that the region encompassed by the entire map extends 5° further south than the other maps in this work to allow the reader to better see the sub-region of interest for the scatter plot data. Blue dots are the model data, the red line is a linear fit for low (<10%) open ocean fraction and the yellow line is a linear fit for open ocean fractions above 10%. Note that the bottom of the region considered is the same as the bottom of the map.

that in Kawai et al. but this is expected since the latter include stratus and fog as well as Sc.

Figure 13(b) shows Sc at the ice edge — Figure 12 solid box— and shows two quite different behaviours above and below an open ocean fraction of $\sim$ 10%. Below 10%, the change in Sc amount increases sharply with a gradient of 0.85 whereas above 10% the increase slows markedly and the gradient is reduced by a factor of $\approx$ 20.

The sharp increase in Sc amount at low open ocean fractions explains the reversal of the correlation between 1.5m temperature and Sc near the ice edge compared to the in and around the AGRIF region. At these higher southern latitudes, the surface albedo is suddenly reduced as the ice starts to melt. This enables evaporation from the now-free ocean surface, thus promoting low cloud formation (Huang et al., 2019). This is the reverse of the behaviour seen elsewhere where - to a first approximation - Sc amount increases with increased southerly latitude (Figure 6(h)).

Finally we examine the r^- regime seasonally in Figure 14 which shows the DJF and JJA model data against the same Kawai et al data and using the same axis limits as Figure 13(a).

For the DJF data — red dots in Figure 14 — show a shift to warmer temperatures as expected for austral summer and a reduced gradient compared to the annual mean temperatures. This means that for a given increase in temperature there is a smaller reduction Sc amount for the summer months. The reverse is true for the JJA data and the difference in gradients for the JJA and DJF data is approximately equal to the range of gradients possible through the Kawai et al. (2017) data which is indicative of the relationship between air temperature and Sc amount being well-captured by the models.

4 Conclusions

In this work we have studied the impact a regional nested ocean model, surrounding New Zealand, has on the ocean-atmosphere feedbacks. This is done by comparing two historical simulations between 1989 - 2008 with (Behrens et al., 2020) and without (Sellar et al., 2019, 2020) a nested, regional ocean model.

The atmospheric temperature response follows that reported in Behrens et al. (2020) for ocean temperature but with less spatial variability; a result of the coarser gridscale in the atmosphere model.

The change in the total cloud amount in the NZESM compared to the UKESM is dominated by changes to stratocumulus and this is strongly negatively correlated with shortwave cloud radiative effect, or SWCRE.

North of $\approx$ -60°S, stratocumulus amount is negatively correlated with air temperature and we refer to this as the r^- regime. This is the case both in the individual simulations as the temperature cools away from the equator — Figure 6 — and when the two models are compared to each other. The gradient of this relationship in the simulations is in close agreement with observations (Kawai et al., 2017) (Figure 13(a)).

The sign of this correlation is reversed near the sea ice edge — the r^+ regime — where a sharp increase in cloud amount is observed as the open ocean fraction increases away from zero. At open ocean fractions above $\approx$ 10%, the gradient decreases markedly, indicating that sudden albedo and evaporation changes dominate the stratocumulus formation processes as the ice starts to melt. This positive correlation has been reported for the Arctic in the previous studies of M. He et al. (2019) and Huang et al. (2019).

Climate models are invariably 'tuned' (Schmidt et al., 2017; Hourdin et al., 2017; McNeall et al., 2020). to minimise various biases. Therefore, making a major change to

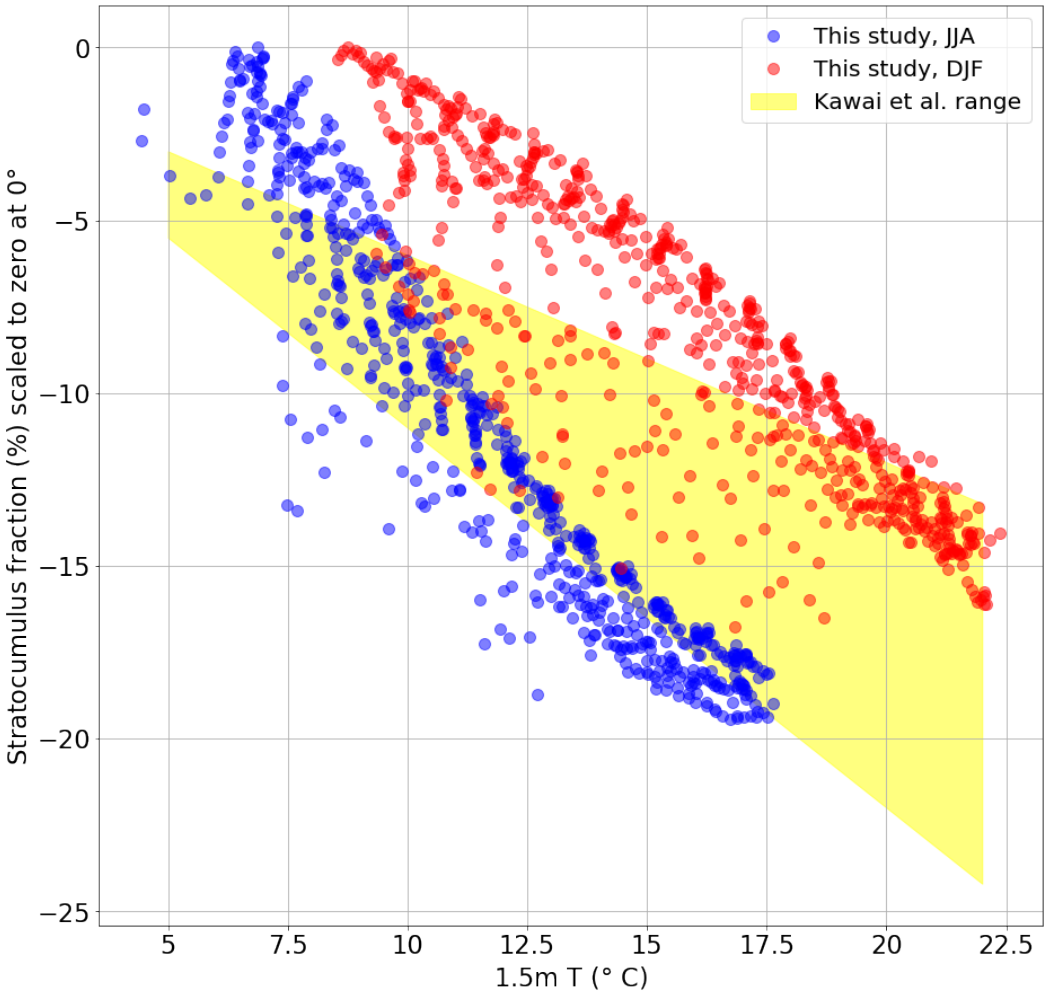

Figure 14. As for Figure 13(a) but for DJF (red) and JJA (blue). The same Kawai et al. (2017) data is shown as in Figure 13.

the regional ocean physics without further tuning, is likely to degrade model performance in some areas. Put another way, some of the bias that the tuning was compensating for is no longer there. This is seen in this study in a deterioration in the SST at high southern latitudes, albeit accompanied by radiative improvements.

In general, clouds and their radiative effects over the Southern Ocean are not well simulated by Earth System Models — see e.g. (Varma et al., 2020; Kuma et al., 2020) — and the changes made here significantly improve the agreement between the simulated and observed shortwave cloud radiative effect, particularly in DJF (Figure 11). The shortwave cloud radiative effect - SWCRE - is negatively correlated with stratocumulus amount (Figure 7,10(b)) and so the general increase in stratocumulus over the Southern Ocean reduces the positive bias compared to CERES-EBAF observations. This improvement is significant between ≈ -60° and -80°S for DJF and annual means where the results lie more than 2 standard deviations from the UKESM historical ensemble mean (Tang et al., 2019) and are hence statistically significant at the 95% level, assuming normally - that is Gaussian - distributed data.

Future work using this nesting methodology on other similarly-related model pairs, as well as this same model pair in different regions of the Southern Ocean – and even elsewhere – would be of significant interest.

Acknowledgments

This paper obtained funding and support through the Ministry of Business Innovation and Employment Deep South National Science Challenge projects (C01X1412) and Royal Society Marsden Fund (NIW1701). The development of the UKESM, was supported by the Met Office Hadley Centre Climate Programme funded by BEIS and Defra (GA01101) and by the Natural Environment Research Council (NERC) national capability grant for the UK Earth System Modelling project, grant number NE/N017951/1.

The authors wish to acknowledge the use of New Zealand eScience Infrastructure (NeSI) high performance computing facilities, consulting support and training services as part of this research. New Zealand's national facilities are provided by NeSI and funded jointly by NeSI's collaborator institutions and through the Ministry of Business, Innovation & Employment's Research Infrastructure programme, www.nesi.org.nz.

The model output of the NZESM (`u-bl274` Met Office identifier) and UKESM (`u-bm456` Met Office identifier) used for the manuscript is publicly available via Zenodo (https://doi.org/10.5281/zenodo.6534266). The model code for NZESM (NEMO + CICE) is publicly available online (https://doi.org/10.5281/zenodo.3873691).

UKESM historical ensemble data is publicly available from the CMIP6 data archive at https://pcmdi.llnl.gov/CMIP6/. The DOI identifier for the ensemble is https://doi.org/10.22033/ESGF/CMIP6.6113. The ensemble members used were `r1i1p1f2`, `r2i1p1f2`, `r3i1p1f2`, `r4i1p1f2`, `r5i1p1f2`, `r6i1p1f2`, `r7i1p1f2`, `r8i1p1f2`, `r9i1p1f2`, `r10i1p1f2`, `r11i1p1f2`, `r12i1p1f2`, `r16i1p1f2`, `r17i1p1f2`, `r18i1p1f2` and `r19i1p1f2`.

ERA5 data is publicly available from https://www.ecmwf.int/en/forecasts/datasets/reanalysis-datasets/era5.

ISCCP data is publicly available from https://www.ncdc.noaa.gov/isccp/isccp-data-access/isccp-data.

CERES-EBAF data is publicly available from https://ceres.larc.nasa.gov/data/.

References

Archibald, A. T., O'Connor, F. M., Abraham, N. L., Archer-Nicholls, S., Chipperfield, M. P., Dalvi, M., ... Zeng, G. (2020). Description and evaluation of the UKCA stratosphere–troposphere chemistry scheme (StratTrop vn 1.0) implemented in UKESM1. *Geoscientific Model Development*, *13*(3), 1223–1266. Retrieved from https://gmd.copernicus.org/articles/13/1223/2020/ doi: 10.5194/gmd-13-1223-2020

Behrens, E. (2020). *erikbehrens/NZESM1: First release of the NZESM (ocean+sea ice code).* Zenodo. Retrieved from https://doi.org/10.5281/zenodo.3873691 doi: 10.5281/zenodo.3873691

Behrens, E., Williams, J., Morgenstern, O., Sutton, P., Rickard, G., & Williams, M. J. (2020). Local grid refinement in New Zealand's earth system model: Tasman Sea ocean circulation improvements and super-gyre circulation implications. *Journal of Advances in Modeling Earth Systems*, *12*(7), e2019MS001996.

Bodas-Salcedo, A., Hill, P. G., Furtado, K., Williams, K. D., Field, P. R., Manners, J. C., ... Kato, S. (2016, May). Large contribution of supercooled liquid clouds to the Solar Radiation budget of the Southern Ocean. *Journal of Climate*, *29*(11), 4213–4228. Retrieved from https://doi.org/10.1175%2Fjcli-d-15-0564.1 doi: 10.1175/jcli-d-15-0564.1

Bodas-Salcedo, A., Williams, K. D., Field, P. R., & Lock, A. P. (2012, November). The surface downwelling solar radiation surplus over the southern ocean in the met office model: The role of midlatitude cyclone clouds. *Journal of Climate*, *25*(21), 7467–7486. Retrieved from https://doi.org/10.1175%2Fjcli-d-11-00702.1 doi: 10.1175/jcli-d-11-00702.1

Brown, A., Beare, R., Edwards, J., Lock, A., Keogh, S., Milton, S., & Walters, D. (2008). Upgrades to the boundary-layer scheme in the met office numerical weather prediction model. *Boundary-Layer Meteorology*, *128*(1), 117–132.

Brown, A., Milton, S., Cullen, M., Golding, B., Mitchell, J., & Shelly, A. (2012). Unified modeling and prediction of weather and climate: A 25-year journey. *Bulletin of the American Meteorological Society*, *93*(12), 1865 - 1877. Retrieved from https://journals.ametsoc.org/view/journals/bams/93/12/bams-d-12-00018.1.xml doi: 10.1175/BAMS-D-12-00018.1

Chassignet, E. P., Yeager, S. G., Fox-Kemper, B., Bozec, A., Castruccio, F., Danabasoglu, G., ... Xu, X. (2020). Impact of horizontal resolution on global ocean–sea ice model simulations based on the experimental protocols of the Ocean Model Intercomparison Project phase 2 (OMIP-2). *Geoscientific Model Development*, *13*(9), 4595–4637. Retrieved from https://gmd.copernicus.org/articles/13/4595/2020/ doi: 10.5194/gmd-13-4595-2020

Craig, A., Valcke, S., & Coquart, L. (2017). Development and performance of a new version of the oasis coupler, oasis3-mct_3.0. *Geoscientific Model Development*, *10*(9), 3297–3308. Retrieved from https://gmd.copernicus.org/articles/10/3297/2017/ doi: 10.5194/gmd-10-3297-2017

Debreu, L., Vouland, C., & Blayo, E. (2008). AGRIF: Adaptive grid refinement in fortran. *Computers & Geosciences*, *34*(1), 8–13.

Edwards, J. M., & Slingo, A. (1996). Studies with a flexible new radiation code. i: Choosing a configuration for a large-scale model. *Quarterly Journal of the Royal Meteorological Society*, *122*(531), 689-719. Retrieved from https://rmets.onlinelibrary.wiley.com/doi/abs/10.1002/qj.49712253107 doi: https://doi.org/10.1002/qj.49712253107

Eyring, V., Bony, S., Meehl, G. A., Senior, C. A., Stevens, B., Stouffer, R. J., & Taylor, K. E. (2016, May). Overview of the coupled model intercomparison project phase 6 (CMIP6) experimental design and organization. *Geoscientific Model Development*, *9*(5), 1937–1958. Retrieved from https://doi.org/10.5194%2Fgmd-9-1937-2016 doi: 10.5194/gmd-9-1937-2016

Good, S. A., Martin, M. J., & Rayner, N. A. (2013). EN4: Quality controlled ocean temperature and salinity profiles and monthly objective analyses with uncertainty estimates. *Journal of Geophysical Research: Oceans*, *118*(12), 6704–6716.

Gregory, D., & Rowntree, P. R. (1990). A mass flux convection scheme with representation of cloud ensemble characteristics and stability-dependent closure. *Monthly Weather Review*, *118*(7), 1483 - 1506. Retrieved from https://journals.ametsoc.org/view/journals/mwre/118/7/1520-0493_1990_118_1483_amfcsw_2_0_co_2.xml doi: 10.1175/1520-0493(1990)118⟨1483:AMFCSW⟩2.0.CO;2

Hawcroft, M., Haywood, J. M., Collins, M., Jones, A., Jones, A. C., & Stephens, G. (2016, June). Southern ocean albedo, inter-hemispheric energy transports and the double ITCZ: global impacts of biases in a coupled model. *Climate Dynamics*, *48*(7-8), 2279–2295. Retrieved from https://doi.org/10.1007%2Fs00382-016-3205-5 doi: 10.1007/s00382-016-3205-5

He, J., Kirtman, B., Soden, B. J., Vecchi, G. A., Zhang, H., & Winton, M. (2018). Impact of ocean eddy resolution on the sensitivity of precipitation to CO_2 increase. *Geophysical Research Letters*, *45*(14), 7194-7203. Retrieved from https://agupubs.onlinelibrary.wiley.com/doi/abs/10.1029/2018GL078235 doi: https://doi.org/10.1029/2018GL078235

He, M., Hu, Y., Chen, N., Wang, D., Huang, J., & Stamnes, K. (2019, July). High cloud coverage over melted areas dominates the impact of clouds on the albedo feedback in the Arctic. *Scientific Reports*, *9*(1). Retrieved from https://doi.org/10.1038%2Fs41598-019-44155-w doi: 10.1038/s41598-019-44155-w

Hersbach, H., Bell, B., Berrisford, P., Hirahara, S., Horányi, A., Muñoz-Sabater, J., ... others (2020). The ERA5 global reanalysis. *Quarterly Journal of the Royal Meteorological Society*, *146*(730), 1999–2049.

Hourdin, F., Mauritsen, T., Gettelman, A., Golaz, J.-C., Balaji, V., Duan, Q., ... Williamson, D. (2017, March). The art and science of climate model tuning. *Bulletin of the American Meteorological Society*, *98*(3), 589–602. Retrieved from https://doi.org/10.1175%2Fbams-d-15-00135.1 doi: 10.1175/bams-d-15-00135.1

Huang, Y., Dong, X., Bailey, D. A., Holland, M. M., Xi, B., DuVivier, A. K., ... Deng, Y. (2019, June). Thicker clouds and accelerated arctic sea ice decline: The atmosphere-sea ice interactions in spring. *Geophysical Research Letters*, *46*(12), 6980–6989. Retrieved from https://doi.org/10.1029%2F2019gl082791 doi: 10.1029/2019gl082791

Hyder, P., Edwards, J. M., Allan, R. P., Hewitt, H. T., Bracegirdle, T. J., Gregory, J. M., ... Belcher, S. E. (2018, September). Critical southern ocean climate model biases traced to atmospheric model cloud errors. *Nature Communications*, *9*(1). Retrieved from https://doi.org/10.1038%2Fs41467-018-05634-2 doi: 10.1038/s41467-018-05634-2

Kawai, H., Koshiro, T., & Webb, M. J. (2017, November). Interpretation of factors controlling low cloud cover and low cloud feedback using a unified predictive index. *Journal of Climate*, *30*(22), 9119–9131. Retrieved from https://doi.org/10.1175%2Fjcli-d-16-0825.1 doi: 10.1175/jcli-d-16-0825.1

Kay, J. E., Wall, C., Yettella, V., Medeiros, B., Hannay, C., Caldwell, P., & Bitz, C. (2016, June). Global climate impacts of fixing the southern ocean shortwave radiation bias in the community earth system model (CESM). *Journal of Climate*, *29*(12), 4617–4636. Retrieved from https://doi.org/10.1175%2Fjcli-d-15-0358.1 doi: 10.1175/jcli-d-15-0358.1

Klein, S. A., & Hartmann, D. L. (1993). The seasonal cycle of low stratiform clouds. *Journal of Climate*, *6*(8), 1587–1606.

Kuhlbrodt, T., Jones, C. G., Sellar, A., Storkey, D., Blockley, E., Stringer, M., ... Walton, J. (2018). The low-resolution version of HadGEM3 GC3.1:

Development and Evaluation for Global Climate. *Journal of Advances in Modeling Earth Systems*, *10*(11), 2865-2888. Retrieved from https://agupubs.onlinelibrary.wiley.com/doi/abs/10.1029/2018MS001370 doi: https://doi.org/10.1029/2018MS001370

Kuma, P., McDonald, A. J., Morgenstern, O., Alexander, S. P., Cassano, J. J., Garrett, S., ... Williams, J. (2020, June). Evaluation of Southern Ocean cloud in the HadGEM3 general circulation model and MERRA-2 reanalysis using ship-based observations. *Atmospheric Chemistry and Physics*, *20*(11), 6607–6630. Retrieved from https://doi.org/10.5194%2Facp-20-6607-2020 doi: 10.5194/acp-20-6607-2020

Kwok, R., & Rothrock, D. A. (2009). Decline in arctic sea ice thickness from submarine and icesat records: 1958–2008. *Geophysical Research Letters*, *36*(15). Retrieved from https://agupubs.onlinelibrary.wiley.com/doi/abs/10.1029/2009GL039035 doi: https://doi.org/10.1029/2009GL039035

Loeb, N. G., Doelling, D. R., Wang, H., Su, W., Nguyen, C., Corbett, J. G., ... Kato, S. (2018). Clouds and the earth's radiant energy system (ceres) energy balanced and filled (ebaf) top-of-atmosphere (toa) edition-4.0 data product. *Journal of Climate*, *31*(2), 895–918.

Mace, G. G., Houser, S., Benson, S., Klein, S. A., & Min, Q. (2011, March). Critical evaluation of the ISCCP simulator using ground-based remote sensing data. *Journal of Climate*, *24*(6), 1598–1612. Retrieved from https://doi.org/10.1175%2F2010jcli3517.1 doi: 10.1175/2010jcli3517.1

McNeall, D., Williams, J., Betts, R., Booth, B., Challenor, P., Good, P., & Wiltshire, A. (2020, May). Correcting a bias in a climate model with an augmented emulator. *Geoscientific Model Development*, *13*(5), 2487–2509. Retrieved from https://doi.org/10.5194%2Fgmd-13-2487-2020 doi: 10.5194/gmd-13-2487-2020

Mulcahy, J. P., Johnson, C., Jones, C. G., Povey, A. C., Scott, C. E., Sellar, A., ... Yool, A. (2020). Description and evaluation of aerosol in UKESM1 and HadGEM3-GC3.1 CMIP6 historical simulations. *Geoscientific Model Development*, *13*(12), 6383–6423. Retrieved from https://gmd.copernicus.org/articles/13/6383/2020/ doi: 10.5194/gmd-13-6383-2020

Rayner, N. A., Parker, D. E., Horton, E. B., Folland, C. K., Alexander, L. V., Rowell, D. P., ... Kaplan, A. (2003). Global analyses of sea surface temperature, sea ice, and night marine air temperature since the late nineteenth century. *Journal of Geophysical Research: Atmospheres*, *108*(D14). Retrieved from https://agupubs.onlinelibrary.wiley.com/doi/abs/10.1029/2002JD002670 doi: https://doi.org/10.1029/2002JD002670

Rossow, W., & Duenas, E. (2004). The international satellite cloud climatology project (ISCCP) web site: An online resource for research. *Bulletin of the American Meteorological Society*, *85*(2), 167–172.

Rossow, W. B., & Schiffer, R. A. (1999). Advances in understanding clouds from ISCCP. *Bulletin of the American Meteorological Society*, *80*(11), 2261–2288.

Sallée, J.-B., Shuckburgh, E., Bruneau, N., Meijers, A. J. S., Bracegirdle, T. J., Wang, Z., & Roy, T. (2013, April). Assessment of southern ocean water mass circulation and characteristics in CMIP5 models: Historical bias and forcing response. *Journal of Geophysical Research: Oceans*, *118*(4), 1830–1844. Retrieved from https://doi.org/10.1002%2Fjgrc.20135 doi: 10.1002/jgrc.20135

Schmidt, G. A., Bader, D., Donner, L. J., Elsaesser, G. S., Golaz, J.-C., Hannay, C., ... Saha, S. (2017, September). Practice and philosophy of climate model tuning across six US modeling centers. *Geoscientific Model Development*, *10*(9), 3207–3223. Retrieved from https://doi.org/10.5194%2Fgmd-10-3207-2017 doi: 10.5194/gmd-10-3207-2017

Sellar, A. A., Jones, C. G., Mulcahy, J. P., Tang, Y., Yool, A., Wiltshire, A., ...

636 others (2019). UKESM1: Description and evaluation of the uk earth system
637 model. *Journal of Advances in Modeling Earth Systems*, *11*(12), 4513–4558.
638 Sellar, A. A., Walton, J., Jones, C. G., Wood, R., Abraham, N. L., Andrejczuk,
639 M., ... Griffiths, P. T. (2020). Implementation of u.k. earth system mod-
640 els for cmip6. *Journal of Advances in Modeling Earth Systems*, *12*(4),
641 e2019MS001946. Retrieved from https://agupubs.onlinelibrary
642 .wiley.com/doi/abs/10.1029/2019MS001946 (e2019MS001946
643 10.1029/2019MS001946) doi: https://doi.org/10.1029/2019MS001946
644 Storkey, D., Blaker, A. T., Mathiot, P., Megann, A., Aksenov, Y., Blockley, E. W.,
645 ... Sinha, B. (2018). UK Global Ocean GO6 and GO7: a traceable hierarchy
646 of model resolutions. *Geoscientific Model Development*, *11*(8), 3187–3213. Re-
647 trieved from https://gmd.copernicus.org/articles/11/3187/2018/ doi:
648 10.5194/gmd-11-3187-2018
649 Swales, D. J., Pincus, R., & Bodas-Salcedo, A. (2018, January). The cloud feed-
650 back model intercomparison project observational simulator package: Version
651 2. *Geoscientific Model Development*, *11*(1), 77–81. Retrieved from https://
652 doi.org/10.5194%2Fgmd-11-77-2018 doi: 10.5194/gmd-11-77-2018
653 Tang, Y., Rumbold, S., Ellis, R., Kelley, D., Mulcahy, J., Sellar, A., ... Jones, C.
654 (2019). *MOHC UKESM1.0-LL model output prepared for CMIP6 CMIP his-*
655 *torical*. Earth System Grid Federation. Retrieved from https://doi.org/
656 10.22033/ESGF/CMIP6.6113 doi: 10.22033/ESGF/CMIP6.6113
657 Taylor, K. E., Stouffer, R. J., & Meehl, G. A. (2012). An overview of cmip5 and
658 the experiment design. *Bulletin of the American meteorological Society*, *93*(4),
659 485–498.
660 Tian, B., & Dong, X. (2020). The double-ITCZ bias in CMIP3, CMIP5, and CMIP6
661 models based on annual mean precipitation. *Geophysical Research Letters*,
662 *47*(8), e2020GL087232.
663 Tsujino, H., Urakawa, L. S., Griffies, S. M., Danabasoglu, G., Adcroft, A. J., Ama-
664 ral, A. E., ... Yu, Z. (2020). Evaluation of global ocean–sea-ice model simula-
665 tions based on the experimental protocols of the Ocean model Intercomparison
666 Project phase 2 (OMIP-2). *Geoscientific Model Development*, *13*(8), 3643–
667 3708. Retrieved from https://gmd.copernicus.org/articles/13/3643/
668 2020/ doi: 10.5194/gmd-13-3643-2020
669 Varma, V., Morgenstern, O., Field, P., Furtado, K., Williams, J., & Hyder, P. (2020,
670 July). Improving the southern ocean cloud albedo biases in a general circula-
671 tion model. *Atmospheric Chemistry and Physics*, *20*(13), 7741–7751. Retrieved
672 from https://doi.org/10.5194%2Facp-20-7741-2020 doi: 10.5194/acp-20
673 -7741-2020
674 Walters, D., Baran, A. J., Boutle, I., Brooks, M., Earnshaw, P., Edwards, J., ...
675 others (2019). The met office unified model global atmosphere 7.0/7.1 and
676 jules global land 7.0 configurations. *Geoscientific Model Development*, *12*(5),
677 1909–1963.
678 Williams, J., Morgenstern, O., Varma, V., Behrens, E., Hayek, W., Oliver, H., ...
679 Frame, D. (2016). Development of the New Zealand Earth System Model.
680 *Weather and Climate*, *36*, 25–44.
681 Wilson, D. R., Bushell, A. C., Kerr-Munslow, A. M., Price, J. D., & Morcrette, C. J.
682 (2008, October). PC2: A prognostic cloud fraction and condensation scheme.
683 I: Scheme description. *Quarterly Journal of the Royal Meteorological Society*,
684 *134*(637), 2093–2107. Retrieved from https://doi.org/10.1002%2Fqj.333
685 doi: 10.1002/qj.333
686 Wilsön, D. R., Bushell, A. C., Kerr-Munslow, A. M., Price, J. D., Morcrette, C. J.,
687 & Bodas-Salcedo, A. (2008, October). PC2: A prognostic cloud fraction
688 and condensation scheme. II: Climate model simulations. *Quarterly Journal*
689 *of the Royal Meteorological Society*, *134*(637), 2109–2125. Retrieved from
690 https://doi.org/10.1002%2Fqj.332 doi: 10.1002/qj.332

Wood, N., Staniforth, A., White, A., Allen, T., Diamantakis, M., Gross, M., ... Thuburn, J. (2014). An inherently mass-conserving semi-implicit semi-lagrangian discretization of the deep-atmosphere global non-hydrostatic equations. *Quarterly Journal of the Royal Meteorological Society*, *140*(682), 1505-1520. Retrieved from https://rmets.onlinelibrary.wiley.com/doi/abs/10.1002/qj.2235 doi: https://doi.org/10.1002/qj.2235

Yool, A., Palmiéri, J., Jones, C. G., de Mora, L., Kuhlbrodt, T., Popova, E. E., ... Sellar, A. A. (2021). Evaluating the physical and biogeochemical state of the global ocean component of UKESM1 in CMIP6 historical simulations. *Geoscientific Model Development*, *14*(6), 3437–3472. Retrieved from https://gmd.copernicus.org/articles/14/3437/2021/ doi: 10.5194/gmd-14-3437-2021

Figure1.

(a) Regional 0.2° circulation strength ($\log_{10}[m \cdot s^{-1}]$)

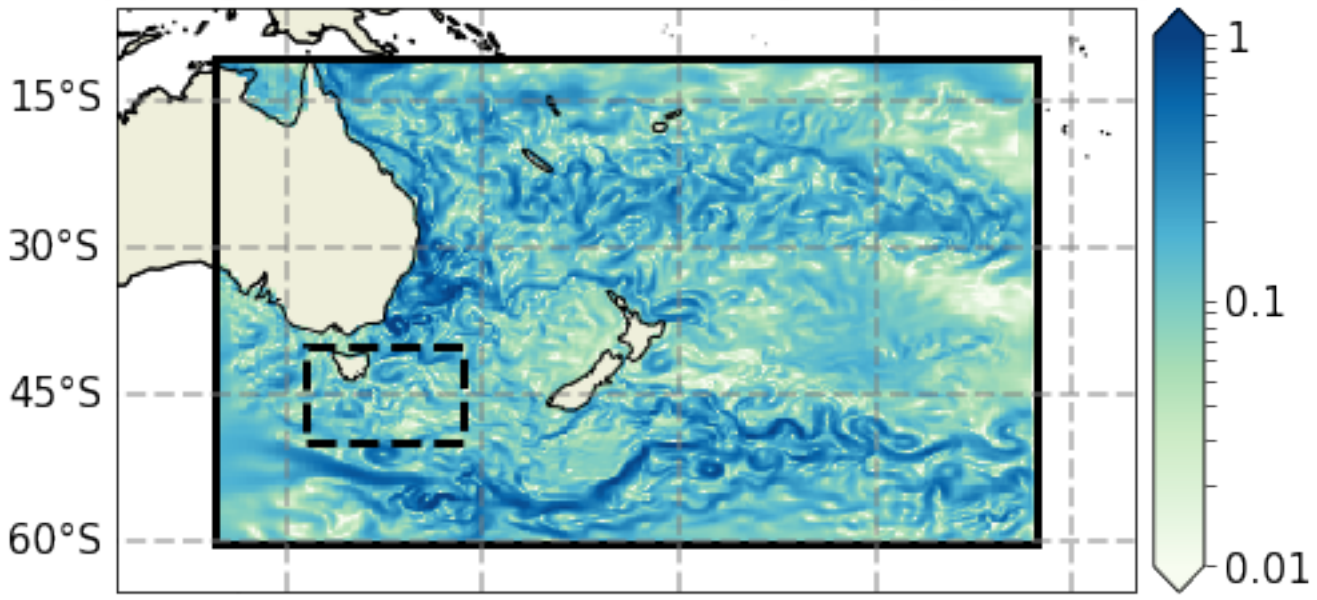

(b) Regional 0.2° circulation strength

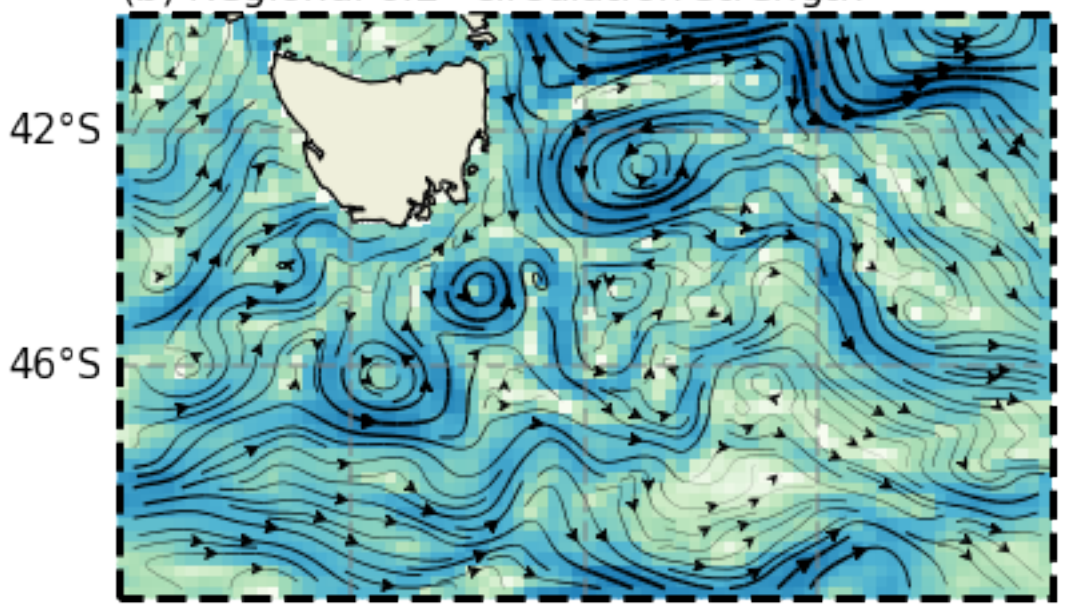

(c) Regional 0.2° SST (°C)

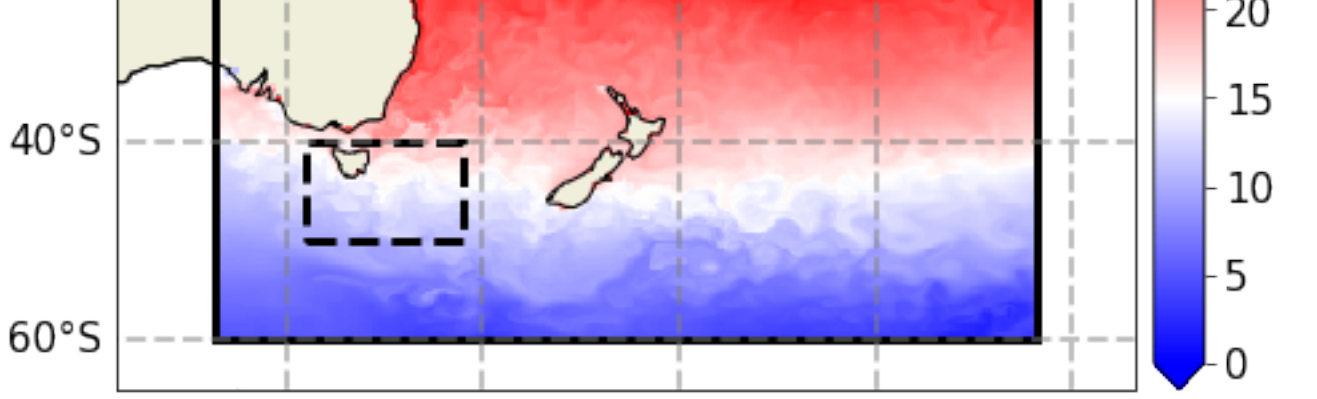

(d) Regional 0.2° SST → from (b)

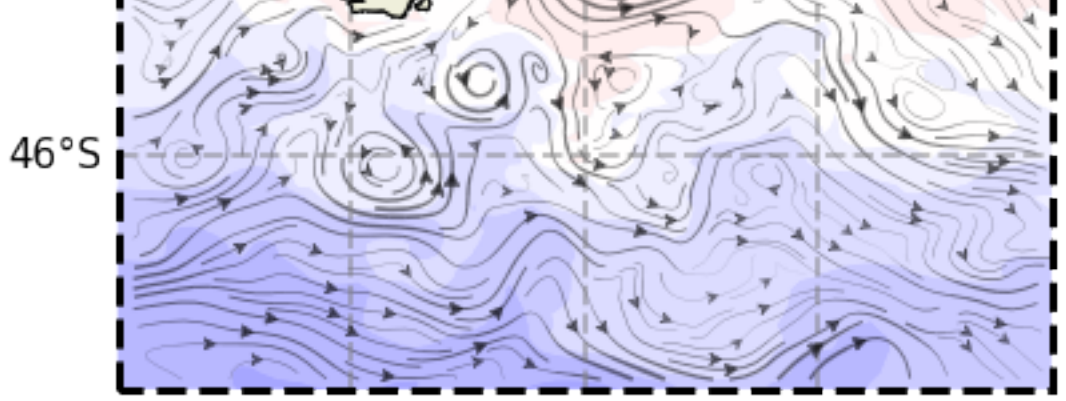

(e) Global 1° SST (°C)

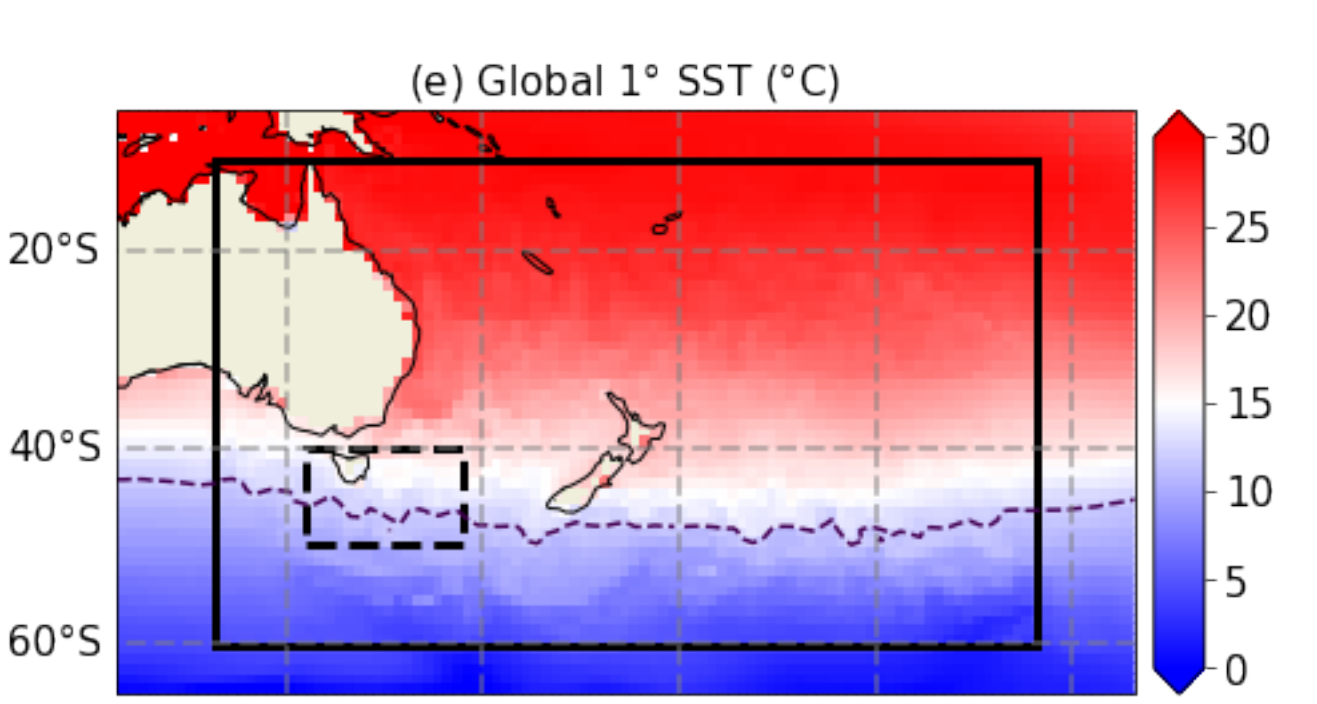

(f) Global 1° SST → from (b)

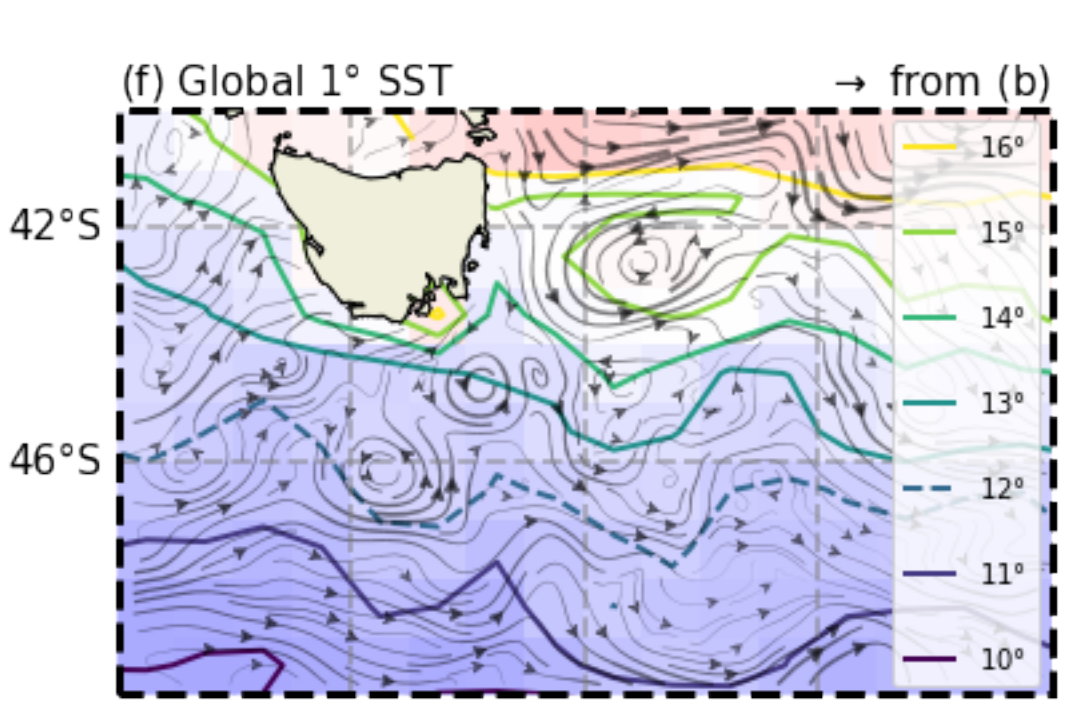

(g) 1.5m air temperature (°C)

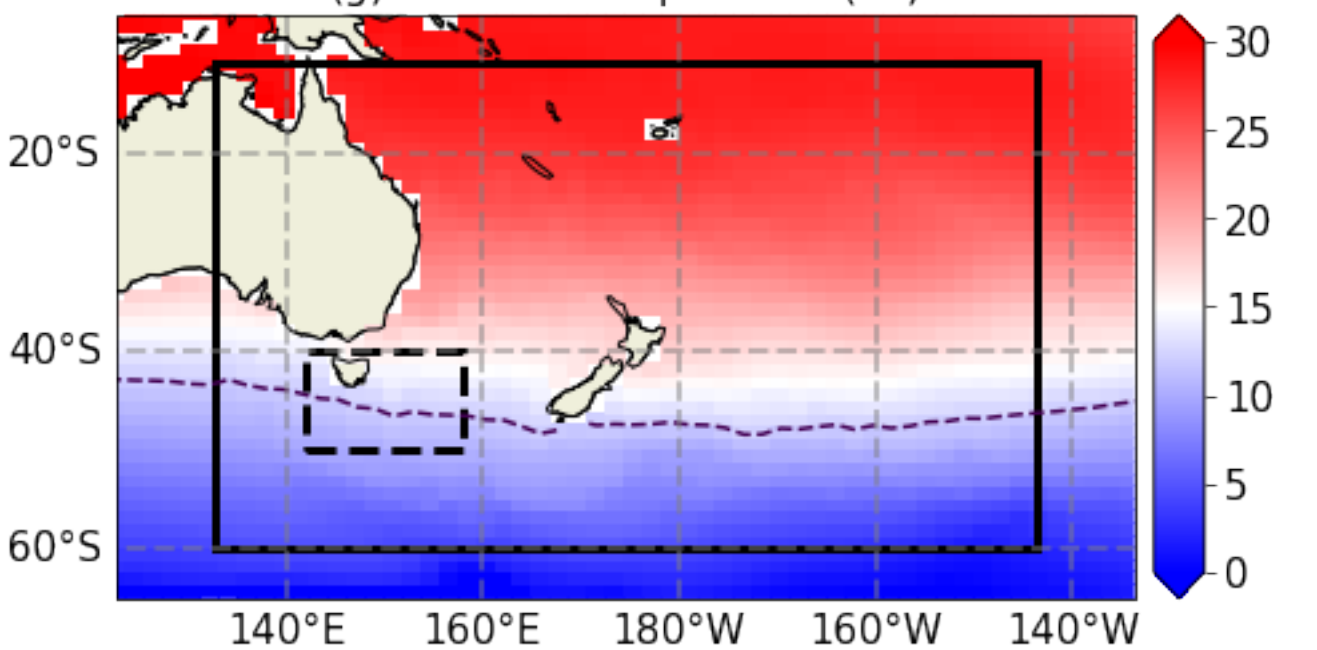

(h) 1.5m air temperature → from (b)

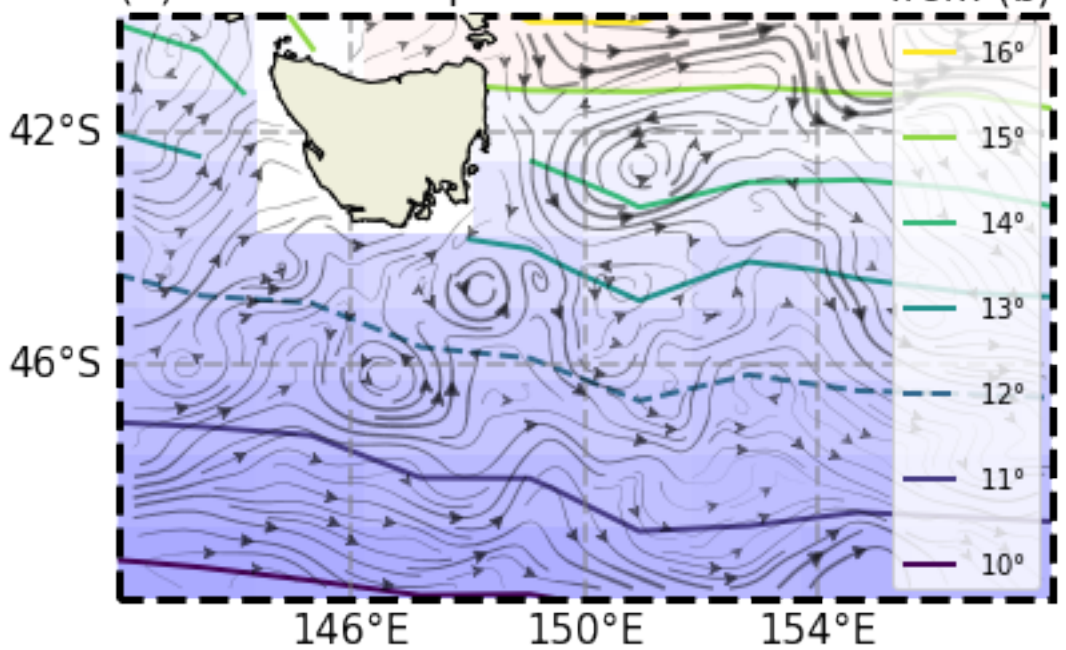

Figure2.

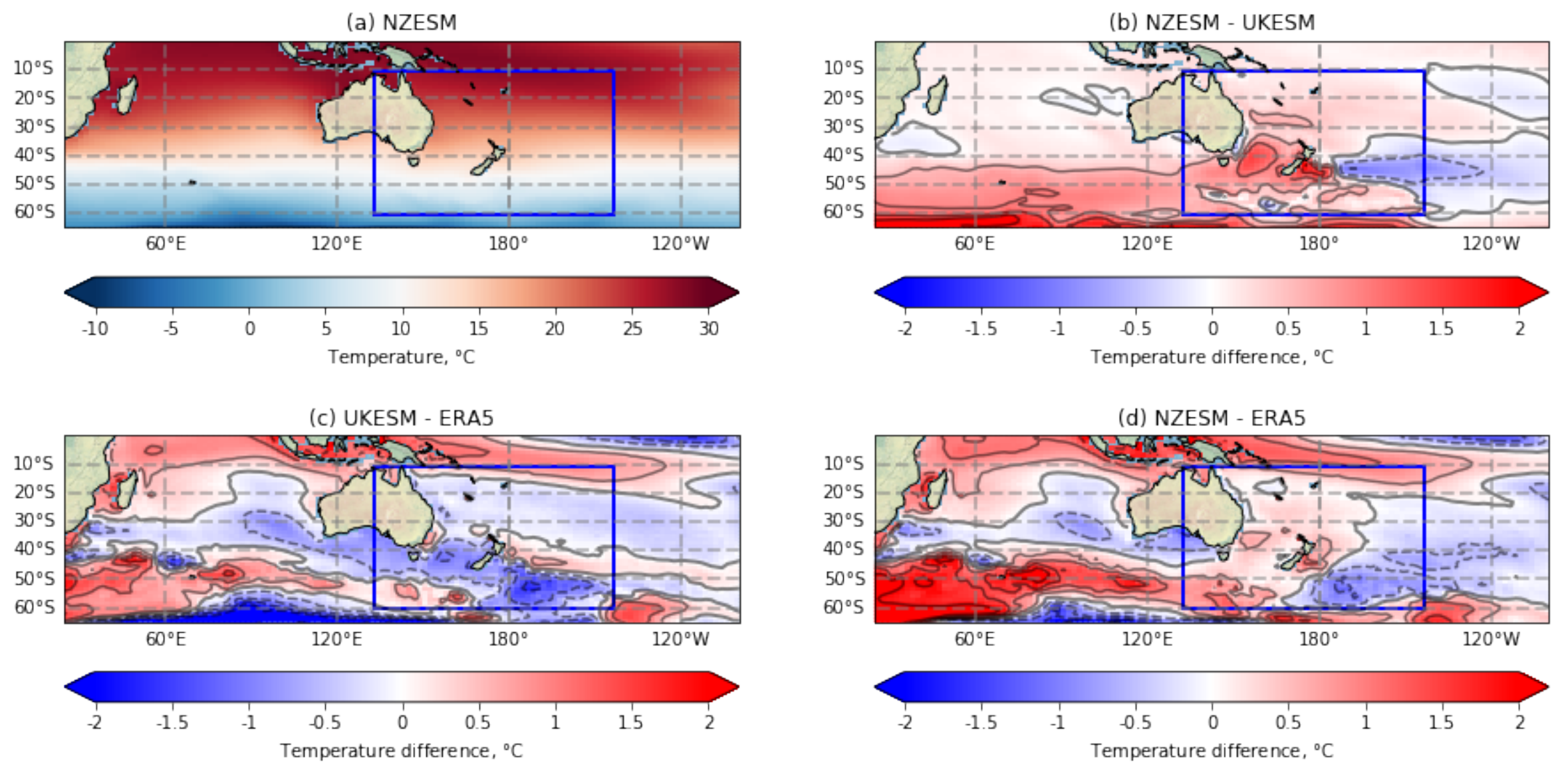
(a) NZESM
10°S
20°S
30°S
40°S
50°S
60°S
60°E
120°E
180°
120°W
-10
-5
0
5
10
15
20
25
30
Temperature, °C
(b) NZESM - UKESM
-2
-1.5
-1
-0.5
0
0.5
1
1.5
2
Temperature difference, °C
(c) UKESM - ERA5
(d) NZESM - ERA5

Figure3.

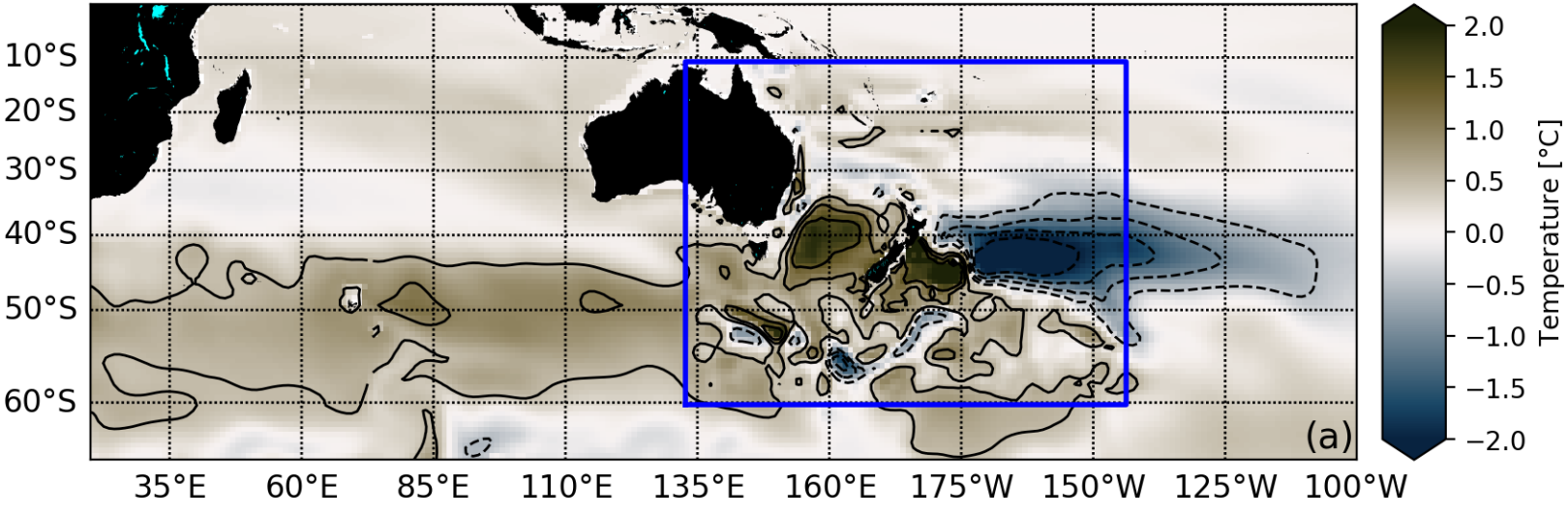
10°S
20°S
30°S
40°S
50°S
60°S
35°E
60°E
85°E
110°E
135°E
160°E
175°W
150°W
125°W
100°W
(a)
2.0
1.5
1.0
0.5
0.0
−0.5
−1.0
−1.5
−2.0
Temperature [°C]

Figure5.

(a) ISCCP cloud amount

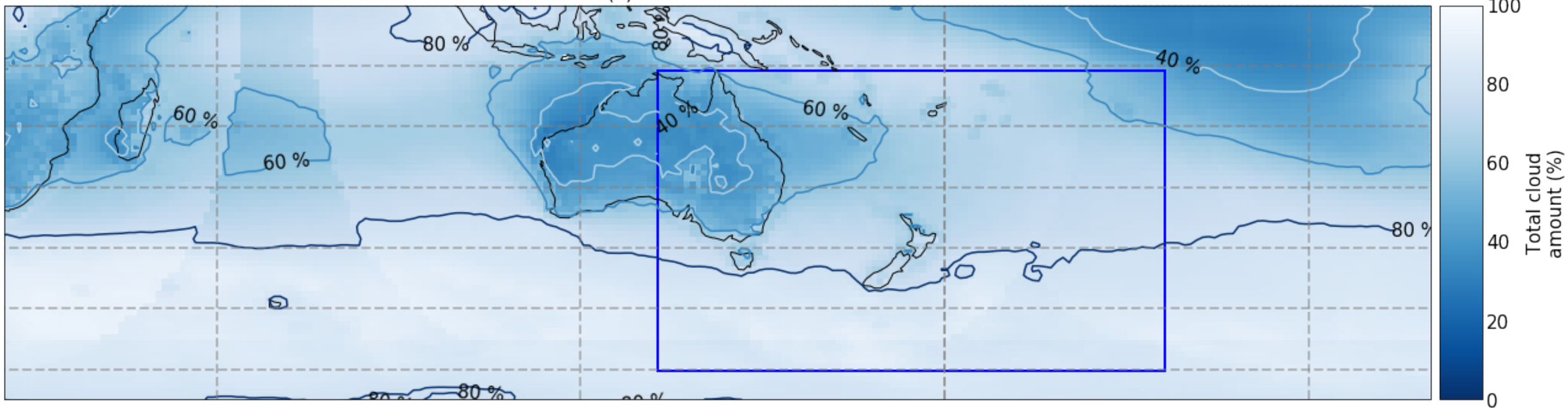

(b) NZESM

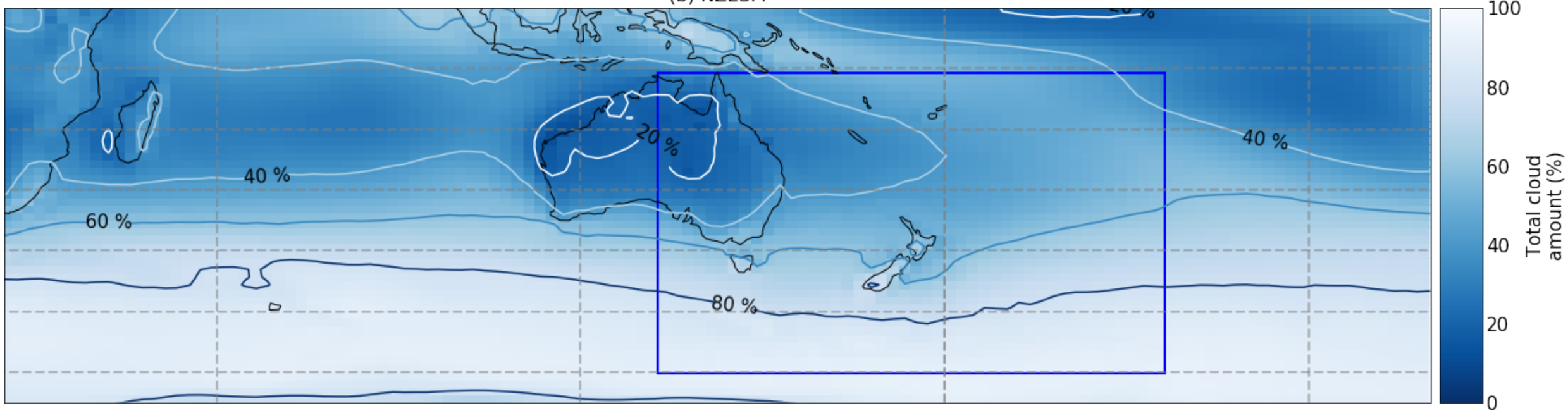

(c) NZESM - UKESM (zero contour marked) and 15% September sea ice cover

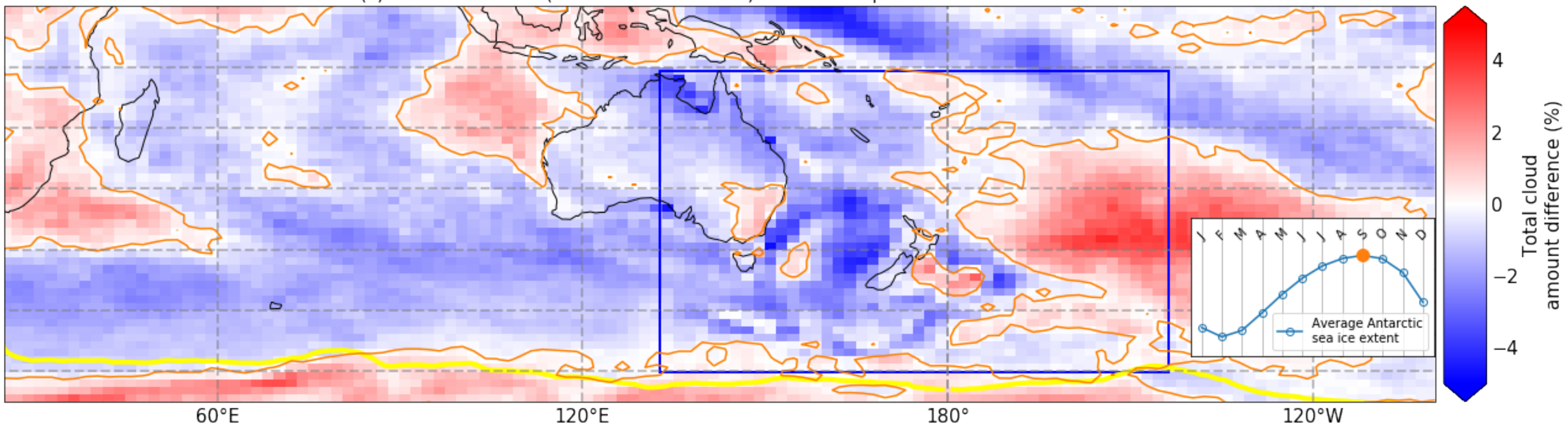

Figure4.

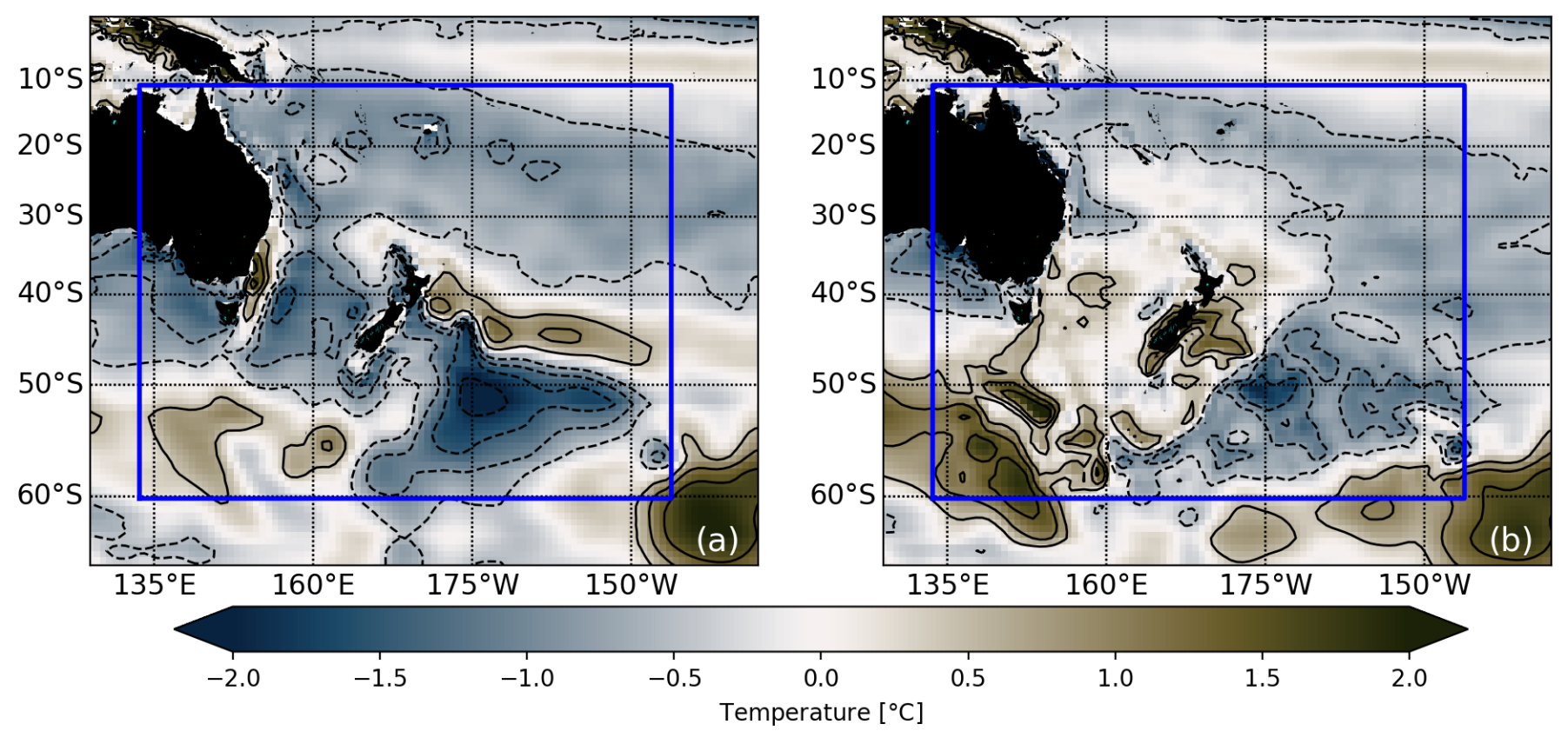
10°S
20°S
30°S
40°S
50°S
60°S
135°E
160°E
175°W
150°W
(a)
(b)
−2.0
−1.5
−1.0
−0.5
0.0
0.5
1.0
1.5
2.0
Temperature [°C]

Figure6.

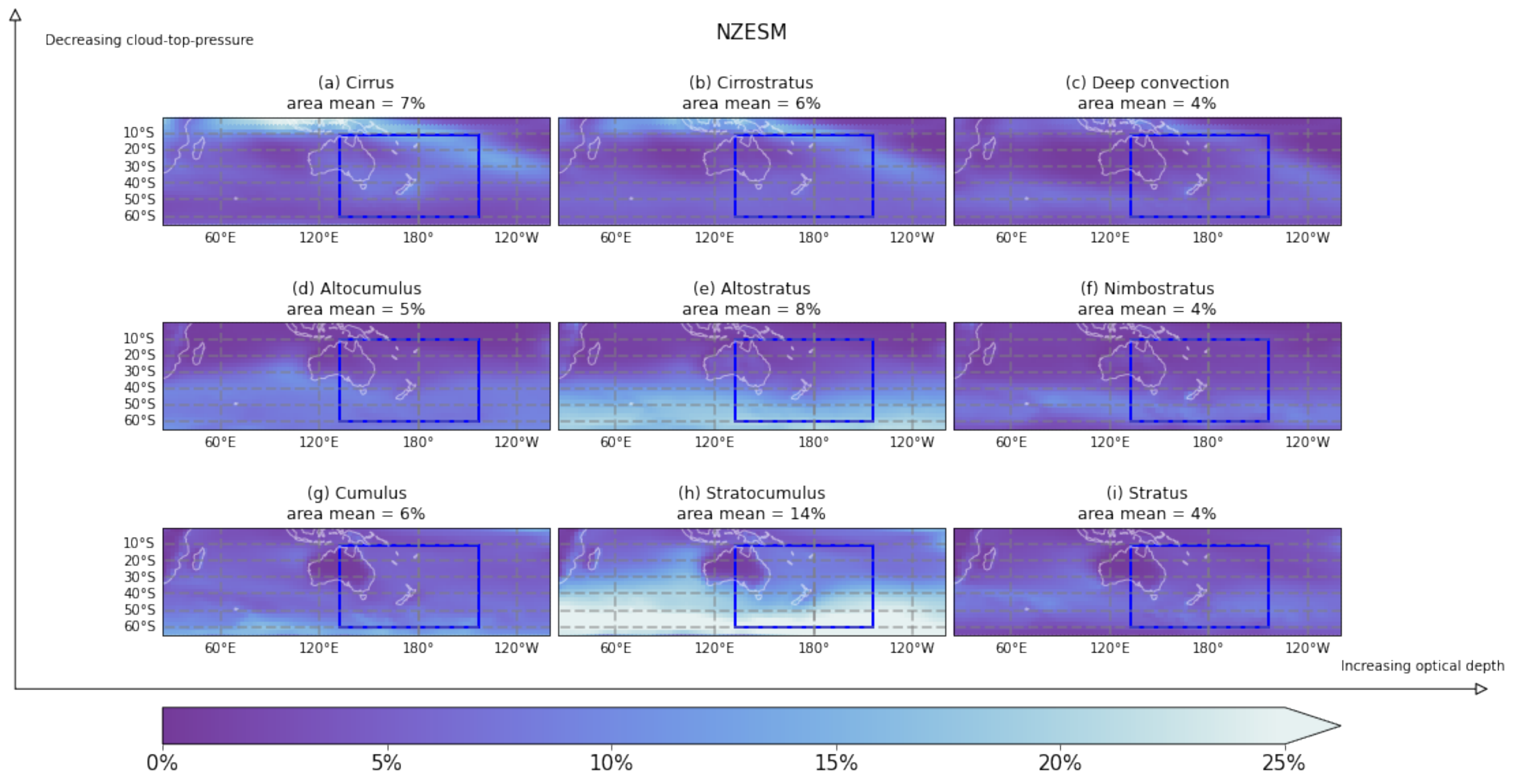
NZESM
Decreasing cloud-top-pressure
(a) Cirrus
area mean = 7%
(b) Cirrostratus
area mean = 6%
(c) Deep convection
area mean = 4%
(d) Altocumulus
area mean = 5%
(e) Altostratus
area mean = 8%
(f) Nimbostratus
area mean = 4%
(g) Cumulus
area mean = 6%
(h) Stratocumulus
area mean = 14%
(i) Stratus
area mean = 4%
10°S
20°S
30°S
40°S
50°S
60°S
60°E
120°E
180°
120°W
Increasing optical depth
0%
5%
10%
15%
20%
25%

Figure7.

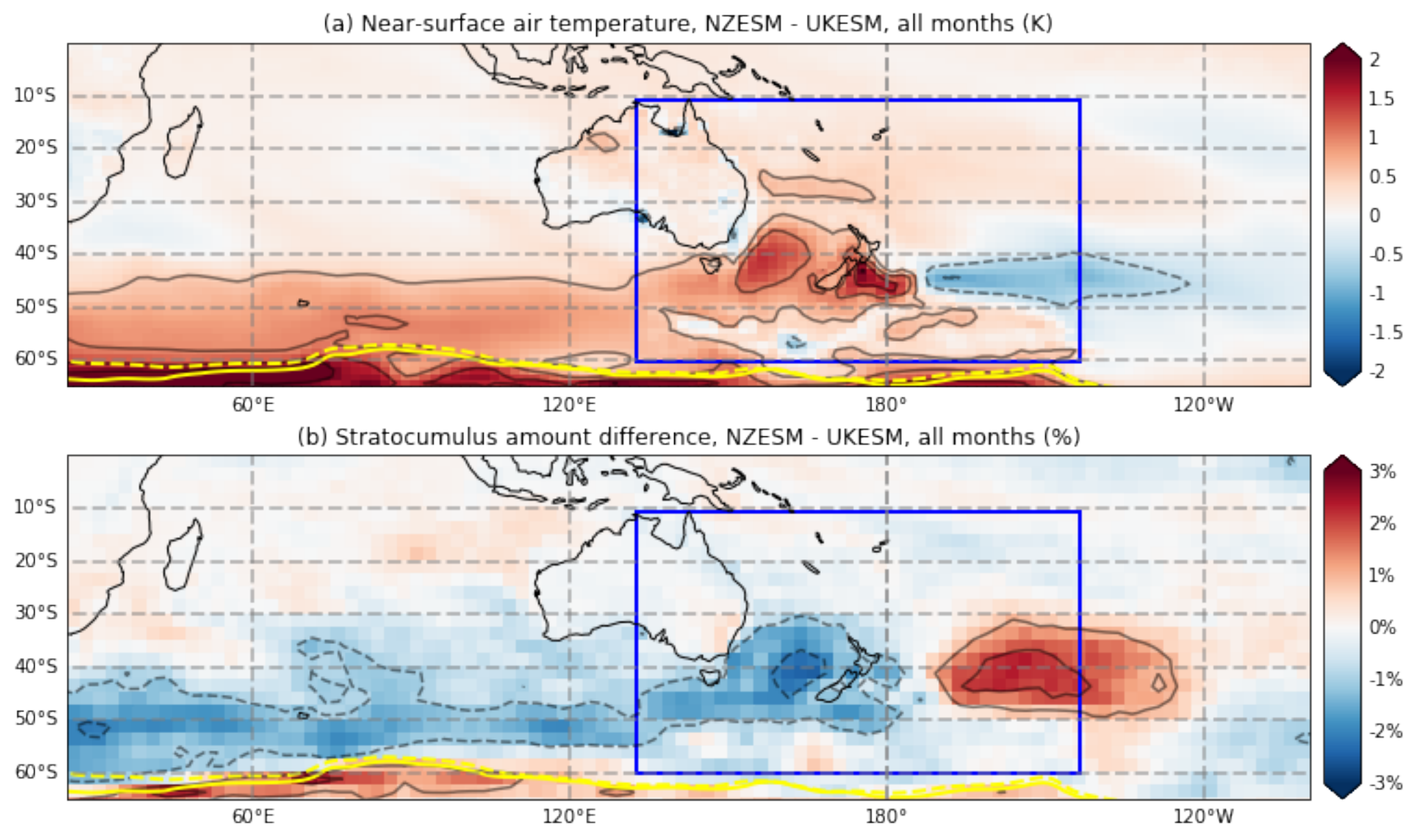
(a) Near-surface air temperature, NZESM - UKESM, all months (K)
10°S
20°S
30°S
40°S
50°S
60°S
60°E
120°E
180°
120°W
2
1.5
1
0.5
0
-0.5
-1
-1.5
-2
(b) Stratocumulus amount difference, NZESM - UKESM, all months (%)
10°S
20°S
30°S
40°S
50°S
60°S
60°E
120°E
180°
120°W
3%
2%
1%
0%
-1%
-2%
-3%

Figure8.

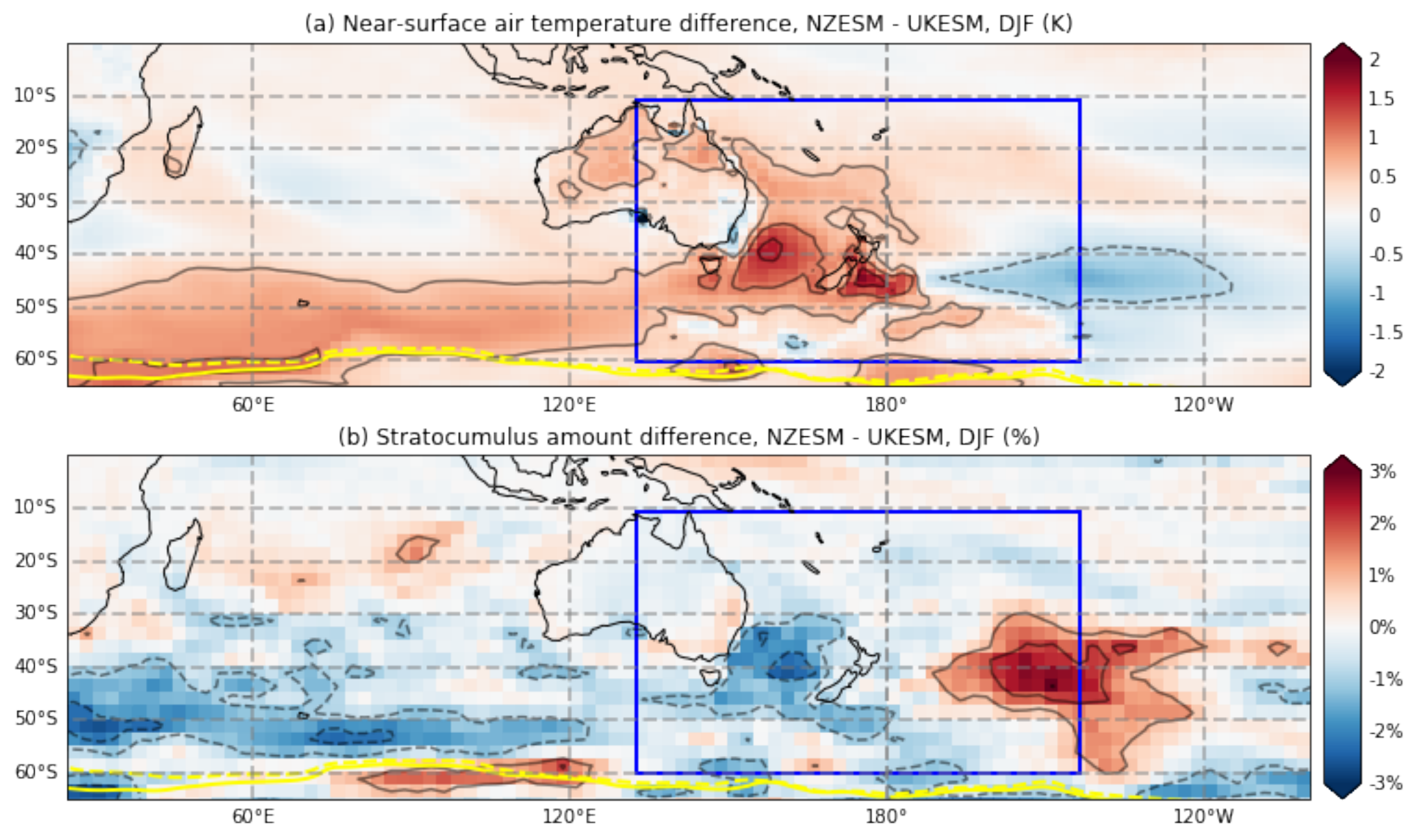
(a) Near-surface air temperature difference, NZESM - UKESM, DJF (K)
10°S
20°S
30°S
40°S
50°S
60°S
60°E
120°E
180°
120°W
2
1.5
1
0.5
0
-0.5
-1
-1.5
-2
(b) Stratocumulus amount difference, NZESM - UKESM, DJF (%)
10°S
20°S
30°S
40°S
50°S
60°S
60°E
120°E
180°
120°W
3%
2%
1%
0%
-1%
-2%
-3%

Figure9.

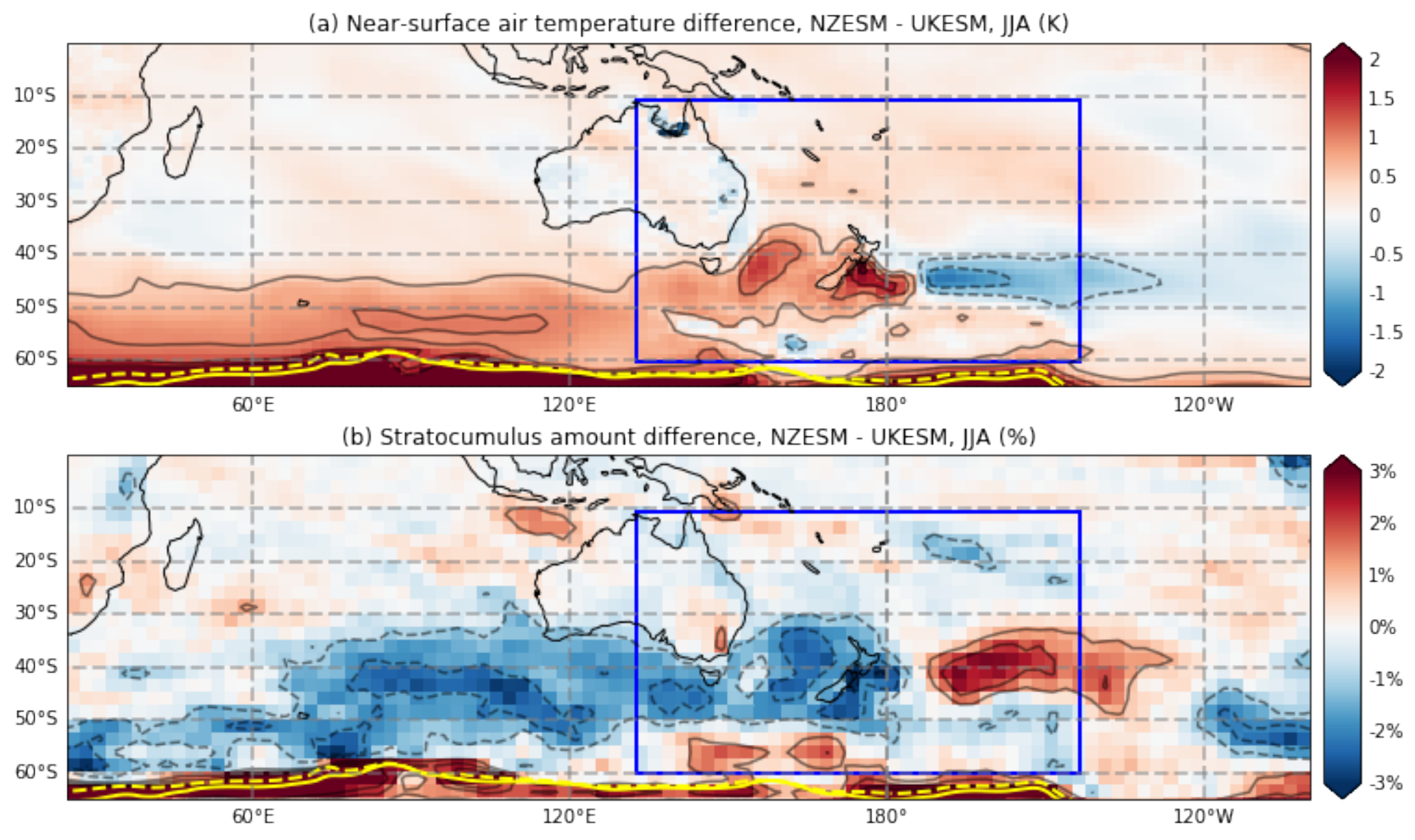
(a) Near-surface air temperature difference, NZESM - UKESM, JJA (K)
10°S
20°S
30°S
40°S
50°S
60°S
60°E
120°E
180°
120°W
2
1.5
1
0.5
0
-0.5
-1
-1.5
-2
(b) Stratocumulus amount difference, NZESM - UKESM, JJA (%)
10°S
20°S
30°S
40°S
50°S
60°S
60°E
120°E
180°
120°W
3%
2%
1%
0%
-1%
-2%
-3%

Figure10.

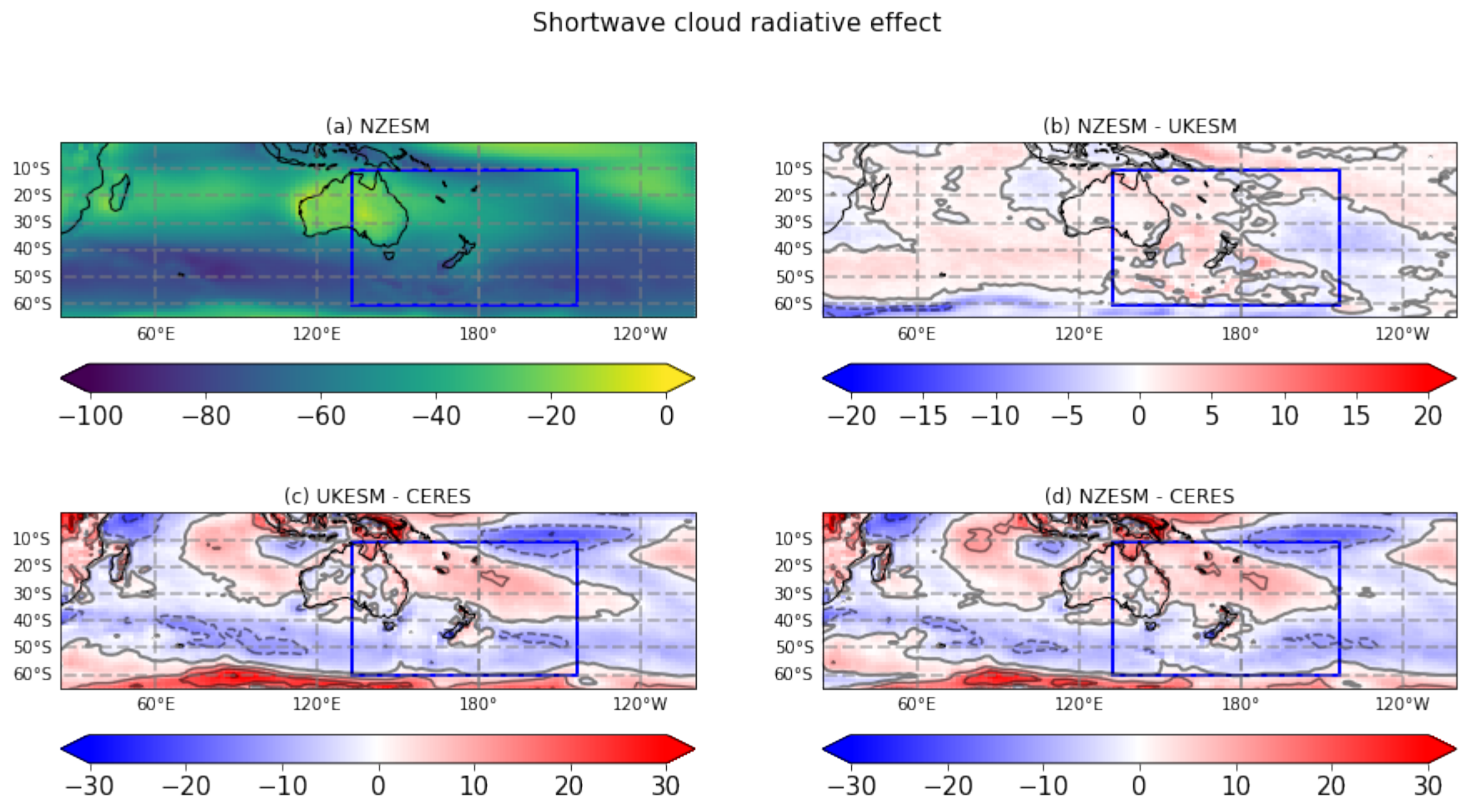
Shortwave cloud radiative effect
(a) NZESM
(b) NZESM - UKESM
(c) UKESM - CERES
(d) NZESM - CERES
10°S
20°S
30°S
40°S
50°S
60°S
60°E
120°E
180°
120°W
−100 −80 −60 −40 −20 0
−20 −15 −10 −5 0 5 10 15 20
−30 −20 −10 0 10 20 30
−30 −20 −10 0 10 20 30

Figure11.

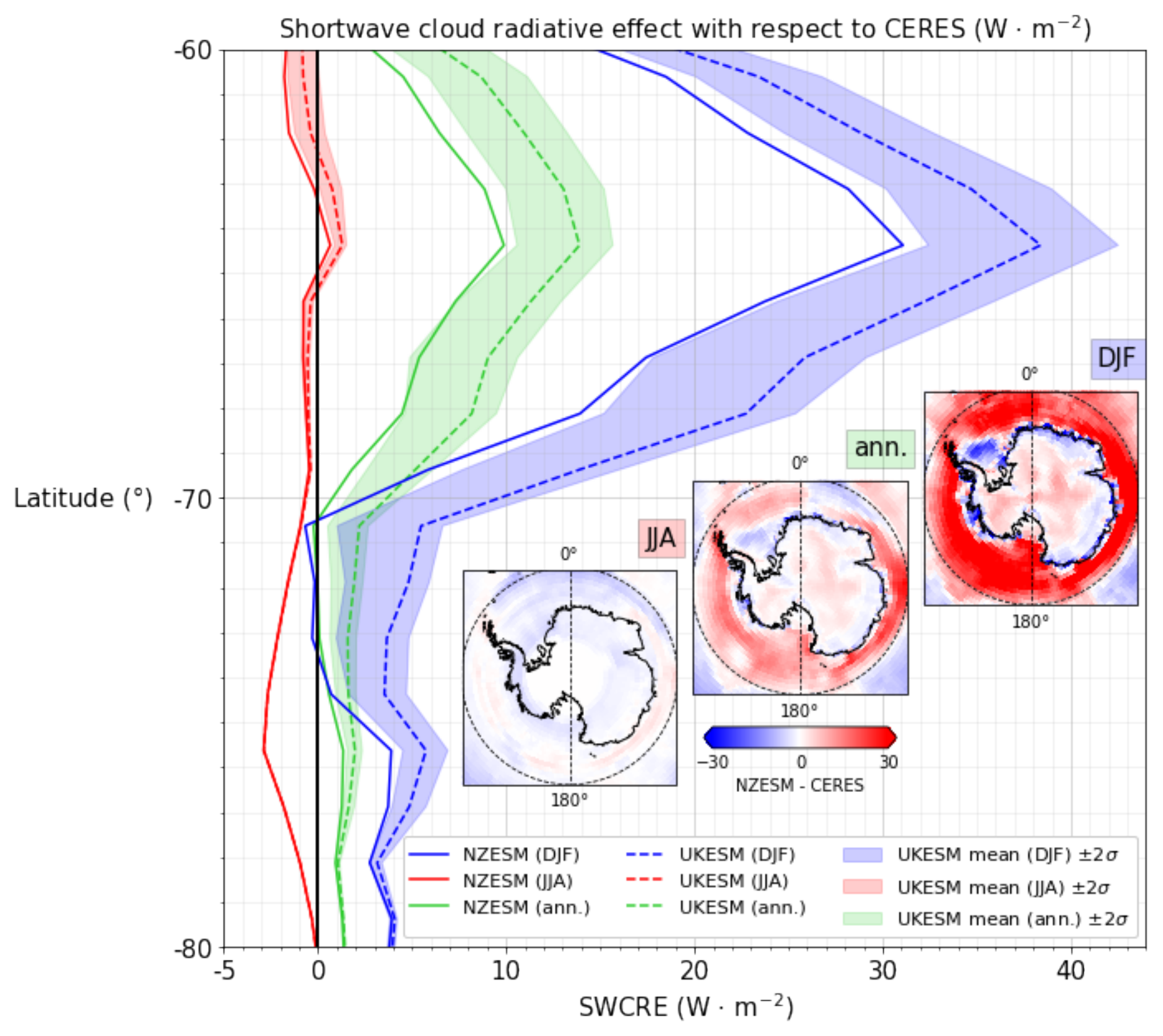
Shortwave cloud radiative effect with respect to CERES (W · m^{-2})
-60
-70
-80
Latitude (°)
-5
0
10
20
30
40
SWCRE (W · m^{-2})
DJF
ann.
JJA
0°
180°
−30
0
30
NZESM - CERES
NZESM (DJF)
NZESM (JJA)
NZESM (ann.)
UKESM (DJF)
UKESM (JJA)
UKESM (ann.)
UKESM mean (DJF) ±2σ
UKESM mean (JJA) ±2σ
UKESM mean (ann.) ±2σ

Figure12.

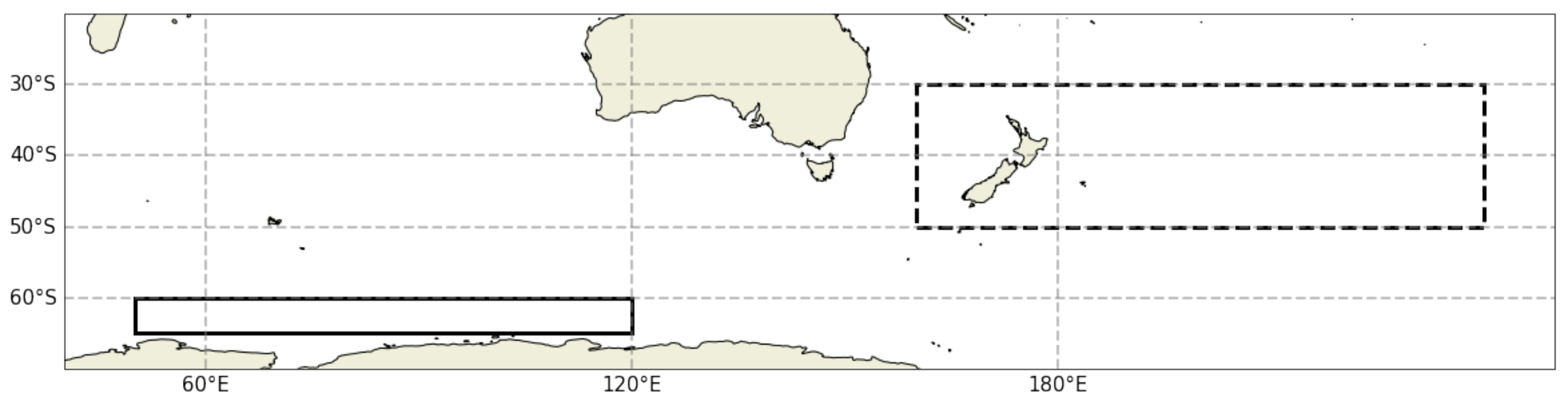
30°S
40°S
50°S
60°S
60°E
120°E
180°E

Figure13.

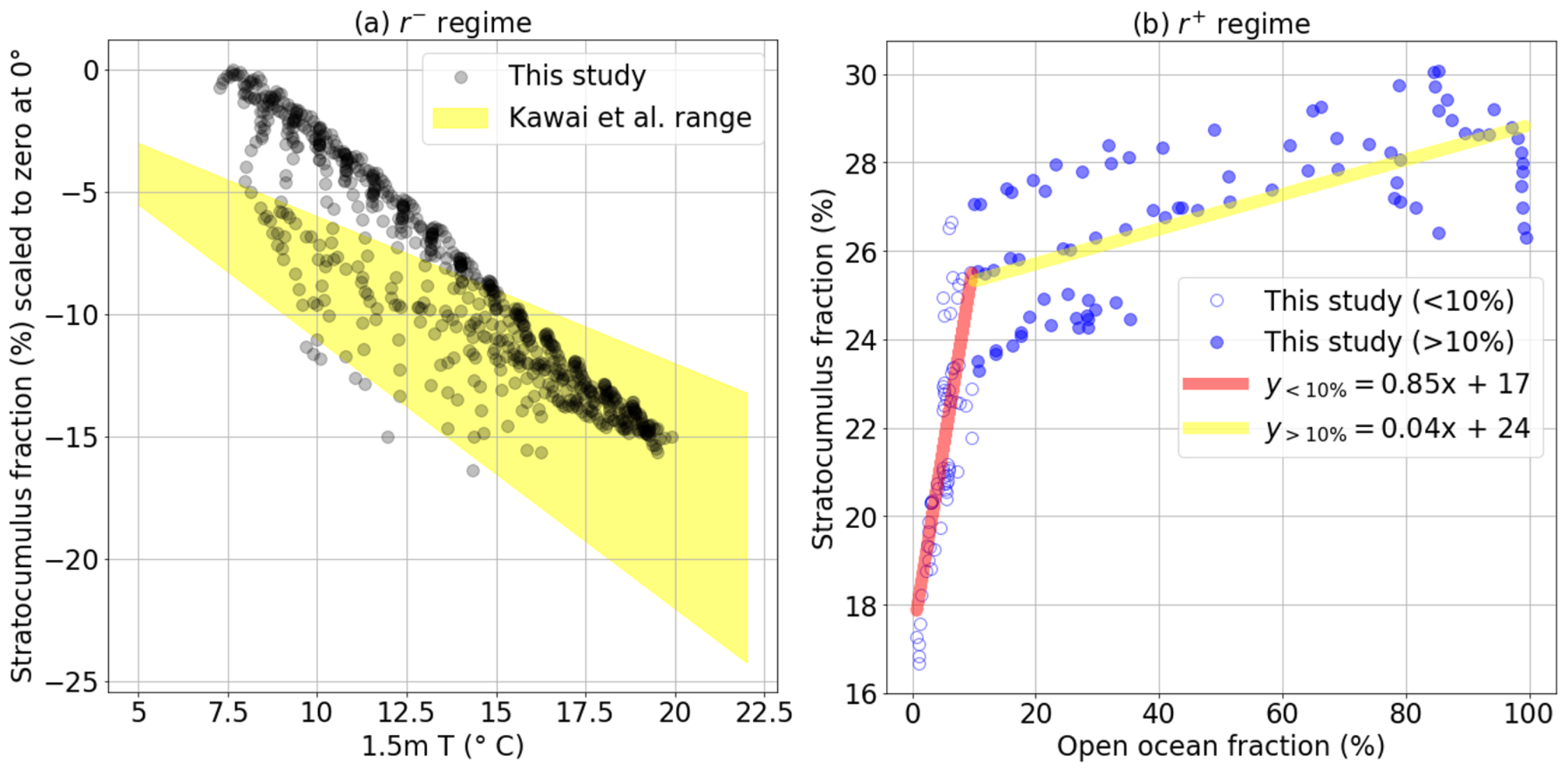
(a) r^- regime
This study
Kawai et al. range
Stratocumulus fraction (%) scaled to zero at 0°
1.5m T (° C)
0
−5
−10
−15
−20
−25
5
7.5
10
12.5
15
17.5
20
22.5
(b) r^+ regime
This study (<10%)
This study (>10%)
$y_{<10\%} = 0.85x + 17$
$y_{>10\%} = 0.04x + 24$
Stratocumulus fraction (%)
Open ocean fraction (%)
30
28
26
24
22
20
18
16
0
20
40
60
80
100

Figure14.

This study, JJA
This study, DJF
Kawai et al. range
0
−5
−10
−15
−20
−25
Stratocumulus fraction (%) scaled to zero at 0°
5
7.5
10
12.5
15
17.5
20
22.5
1.5m T (° C)